Affinity of Telluronium Chalcogen Bond Donors for Lewis Bases in Solution: A Critical Experimental-Theoretical Joint Study

Loïc Groslambert, Yann Cornaton, Matej Ditte, Emmanuel Aubert, Patrick Pale, Alexandre Tkatchenko, Jean-Pierre Djukic, Victor Mamane

Affinity of Telluronium Chalcogen Bond Donors for Lewis Bases in Solution: A Critical Experimental-Theoretical Joint Study

Loïc Groslambert,[a] Yann Cornaton,[b] Matej Ditte,[c] Emmanuel Aubert,[d] Patrick Pale,[a] Alexandre Tkatchenko,[c] Jean-Pierre Djukic,[b,*] and Victor Mamane[a,*]

[a] L. Groslambert, Prof. Dr P. Pale, Dr V. Mamane
LASYROC, UMR 7177 CNRS
University of Strasbourg,
1 Rue Blaise Pascal, F-67000 Strasbourg, France
E-mail: vmamane@unistra.fr

[b] Dr Y. Cornaton, Dr J.-P. Djukic
LCSOM, UMR 7177 CNRS
Université de Strasbourg,
4 rue Blaise Pascal, F-67000 Strasbourg
E-mail: djukic@unistra.fr

[c] M. Ditte, Prof. Dr A. Tkatchenko
Department of Physics and Materials Science
University of Luxembourg,
L-1511 Luxembourg City, Luxembourg

[d] Dr E. Aubert
CNRS, CRM2
University of Lorraine,
F-54000 Nancy, France

Supporting information for this article is given via a link at the end of the document.

Abstract: Telluronium salts $[Ar_2MeTe]X$ were synthesized and their Lewis acidic properties towards a number of Lewis bases were addressed in solution by physical and theoretical means. The structural X-ray diffraction analysis of 21 different salts revealed the electrophilicity of the Te centers in their interactions with anions. Telluroniums' propensity to form Lewis pairs was investigated with $OPPh_3$. Diffusion-ordered NMR spectroscopy suggests that telluroniums may bind up to three $OPPh_3$ molecules. Isotherm titration calorimetry showed that the related heats of association in 1,2-dichloroethane depend on the electronic properties of the substituents of the aryl moiety and on the nature of the counterion. The enthalpies of first association of $OPPh_3$ span -0.5 to -5 kcal/mol. The study of the affinity of telluroniums for $OPPh_3$ by state-of-the-art DFT and *ab initio* methods reveals the dominant Coulombic and dispersion interactions as well as an entropic effect favoring association in solution. Intermolecular orbital interactions between $[Ar_2MeTe]^+$ cations and $OPPh_3$ are deemed insufficient to ensure alone the cohesion of $[Ar_2MeTe{\bullet}B_n]^+$ complexes in solution (B= Lewis base). Comparison of Grimme's and Tkatchenko's DFT-D4 / MBD-vdW thermodynamics of formation of higher $[Ar_2MeTe{\bullet}B_n]^+$ complexes reveals significant molecular size-dependent divergence of the two methodologies, with MBD yielding better agreement with experiment.

Introduction

σ-Hole interactions occur between regions of low electron density observed in halogens, chalcogens and many other bonded atoms (σ-hole donors), and electron-rich partners (σ-hole acceptors).[1-3] Among this class of interactions, the halogen bond (XB) is probably the most prominent regarding its application in many domains.[4] In recent years, the chalcogen bond (ChB) has attracted more attention with important contributions in the context of supramolecular chemistry,[5, 6] crystal engineering[7, 8] and catalysis,[9-13] to name a few. [14, 15] In contrast to halogens in halogenated organic compounds that bear one σ-hole, chalcogens in organic chalcogenides R_2Ch (+II) possess two σ-holes able to participate in σ-hole interactions.[16, 17] If X-ray diffraction (XRD) analysis allows the structural description of such interactions in the crystal,[7] there has been few direct and unambiguous determination of the thermochemistry of ChB association in solution.[18] The latter task can be addressed by complementary means[19] that rely on NMR techniques for establishing the existence of molecular associations in solution, and calorimetric methods such as Isothermal Titration Calorimetry (ITC) to estimate association

enthalpies.[20] Recently, chalconium salts $[R_3Ch]^+$ where the chalcogen(+IV) atom bears three σ-holes have been described as powerful Lewis acid catalysts[21, 22] (Figure 1). Thus, several organic transformations could be efficiently catalyzed with sulfonium,[23, 24] selenonium[25-27] and telluronium[28-33] salts. The latter were also investigated for their ability to transport anions across phospholipid bilayers.[34] While it is clear from these studies that the reactivity of the chalconium salts is based on ChB between the chalcogen(+IV) and the substrate, some questions remain unanswered about the number of σ-holes involved and their behavior in solution.

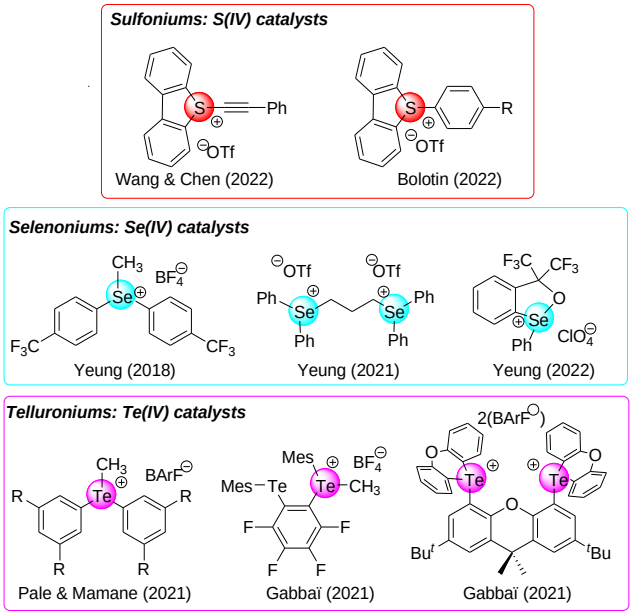

Figure 1. Chalconiums used in organocatalysis ($BArF^-$ = tetrakis(3,5-bis(trifluoromethyl)phenyl)borate).

In other terms, how are these σ-holes occupied in the presence of excess Lewis base in solution ? This information is of utmost importance for the design of active candidates for catalysis and for other solution-based applications.

To date, all the studies performed on adduct formation between chalcogen(II) compounds and Lewis bases in solution considered only the 1:1 stoichiometry.[18, 19] The same stoichiometry was used to describe the association of Lewis bases with diaryliodonium ions, known to behave as organocatalysts[35, 36] although iodine(III) possesses two σ-holes.[37] In these cases the 1:1 stoichiometry is reasonable considering that the first association through one σ-hole should weaken the other.[16] However, different stoichiometry can be expected with atoms bearing up to three σ-holes such as in neutral pnictogen (III) or cationic chalconium(IV) compounds. The binding properties of pnictogen-based species were studied in specific cases[38], showing that $PhSbCl_2$ can bind two chloride anions[39]. Nevertheless, the presence of three σ-holes makes the study in solution rather challenging due to 1) three possible stoichiometries of the adducts with a Lewis base, 2) possible competing interactions between the chalcogen center and interfering Lewis bases (solvent, counterion), and 3) the hardly predictable effects of solvation, such as competing coordination.

Being involved these last years in XB-[40-42] and ChB-catalysis,[19, 43, 44] we have recently reported the high catalytic efficiency of methyldiaryltelluronium salts in various reactions.[28] Herein, in order to gain insight into the interacting ability of diarylmethyltelluroniums in solution, the interaction of various σ-hole acceptors (Lewis bases) with a series of tellurium cations bearing different functional groups and associated with anions of different coordinating ability were addressed by NMR spectroscopy and ITC, complemented by structural XRD analyses and underpinned by state-of-the-art theoretical tools (Figure 2).

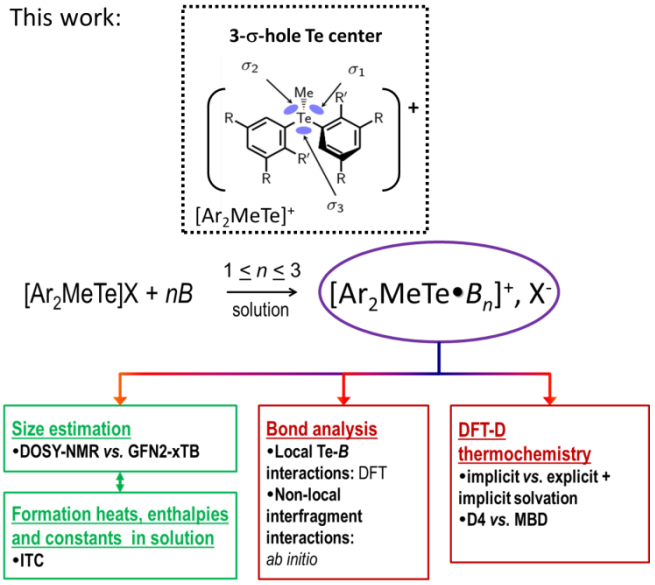

Figure 2. The questions addressed and the methodology used in this study.

The telluronium cations of interest to this study present indeed a marked electrophilicity that was considered particularly suitable for ITC experiments with ChB acceptors,[45] whereas preliminary NMR spectroscopy sensed relatively persistent ChB in solution.[28] While recent reports highlighted the importance of orbital interactions in ChB[46, 47] strength, this study outlines the systemic role of coulombic interactions and dispersion, the crucial influence of solvation in molecular complex formation[48, 49] and questions the very idea of ChB as the main driving force in the formation of molecular complexes in solution.

Results and Discussion

The methodology applied in this study focusses on the extraction of experimental information among which physical observables and their analysis by theoretical means to achieve the most physically sound description of the intermolecular interactions. We therefore adopted a critical and chemical bonding model-"agnostic" or "secular" approach inspired by Clark's recent[50] recommendations, focusing on analyzing with state-of-the-art tools the properties of the electron density topology and considering different models of dispersion correction for their impact on the thermodynamics of association.

The methodology disclosed herein therefore consists of (Figure 2):

1) the synthesis and structural XRD analysis of new telluronium salts and the analysis of Te σ-hole properties in the crystal,

2) the *in solutio* DOSY (diffusion ordered spectroscopy)-NMR investigations of associations between telluronium salts and Lewis bases governed by the establishment of ChB,

3) the ITC-based determination of heats of association in solution and attempts to break down the latter into association enthalpies of first, second and third Lewis base coordination to the Te center,

4) the theoretical analyses of the nature of the interactions involved in the ChB at the local and non-local level by a combination of advanced DFT-D (dispersion)/vdW (van der Waals) and wavefunction theory (WFT) methods backed by robust bond analysis methods, and

5) the evaluation of D/vdW-corrections applied to static DFT, that is the pair-wise[51-55] and many-body[56-58] atomic based corrections, in the challenging computation of the solution thermodynamics of the telluronium-Lewis base association. As shown farther the choice of the proper dispersion/van der Waals corrections in DFT calculations is crucial in modeling the thermodynamics of formation of large molecular aggregates.

The ambition of this study is to demonstrate that only a comprehensive approach (Figure 2), devoid of bonding model preconceptions and focused on the determination of observables and their modeling by theoretical means provides unambiguous answers on the origin of stabilizing interactions responsible for the cohesion of the molecular complexes of interest in vacuum and in solution.

Synthesis of telluronium salts, structural X-ray diffraction (XRD) and electrostatic surface potential (ESP) analyses.

In addition to the previously reported telluronium salts **1a-c**, **2a-c**, **3a-c** and **6a-d**,[28] new derivatives were prepared by varying the electronic or steric properties of the aromatic substituents and the nature of the counterion (Chart 1). Telluroniums **6e-g** were obtained through anion metathesis from the triflate salt **6a** and telluroniums **4a-b**, **5a-b**, **6h**, **7a-b** and **8a-b** were synthesized following reported procedures (see ESI for details). Suitable crystals of **1a**, **1c**, **2a-c**, **3a-c**, **5a**, **6a-b**, **6d-f**, **6h**, **7a-b** and **8a-b** were obtained and only the structures of selected salts are reported in Figure 3.

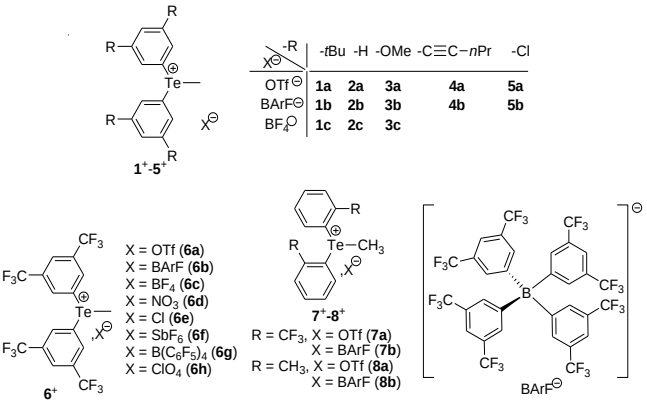

Chart 1. The telluronium salts considered in this work

The structural analysis was complemented by an ESP analysis of the telluronium cations to confirm the formation of ChBs in the solid state and to study the electronic influence of the aromatic substituents on Te σ-holes depth (see ESI for full details). The study focused on the Te•••X interaction by determining its geometrical parameters, the C_{Ar}-Te-*A* angle (θ) and Te-*A* distance (*d*) (*A* represents the acceptor atom). In general, a ChB is defined by θ in the range 160-180° and d below the sum of van der Waals radii of the interacting atoms (Σr_{vdw}). For comparison purposes, the reduction ratio (*RR*) parameter, defined as $d/\Sigma r_{vdw}$, was used. The different values of θ, *d* and *RR* for the telluronium salts are reported in ESI (Table S1), along with the nature of the interacting atom or π region, and their number.

The 21 obtained crystal structures result in 33 crystallographically independent telluronium cations in which the σ-holes (three available per cation) are interacting with a rich acceptor in 88% of the cases. Those acceptors are mostly oxygen (OTf^-, NO_3^-, ClO_4^-) and fluorine (BF_4^-, $BArF^-$) atoms of counteranions and in some cases aromatic carbons atoms of adjacent molecules or fluorine atom on the same Te cation (**7a-b**). For all cases three σ-holes were found for each cation, except for **7a-b** where an intramolecular Te•••F interaction occurs involving one (**7a**) or two (**7b**) σ-holes.[59] For a given *R* substituent on the aryl fragment, the V_{max} potential is more pronounced for σ-holes found in the prolongation of C_{Ar}-Te bonds, the difference being the largest for the most activated cation ($\mathbf{6}^+$: 134.3(2.4) kcal.mol^{-1} for σ(Ar-Te) vs. 129.1(1.1) kcal.mol^{-1} for σ(Me-Te)). The ranking of the mean σ-hole strength is thus $\mathbf{1}^+ < \mathbf{3}^+ < \mathbf{8}^+ < \mathbf{2}^+ < \mathbf{7}^+ < \mathbf{5}^+ < \mathbf{6}^+$, with the exception of σ(Me-Te) of $\mathbf{8}^+$, which is strongly affected by the proximity of *-R* = -Me groups and appears as the least activated σ-hole.

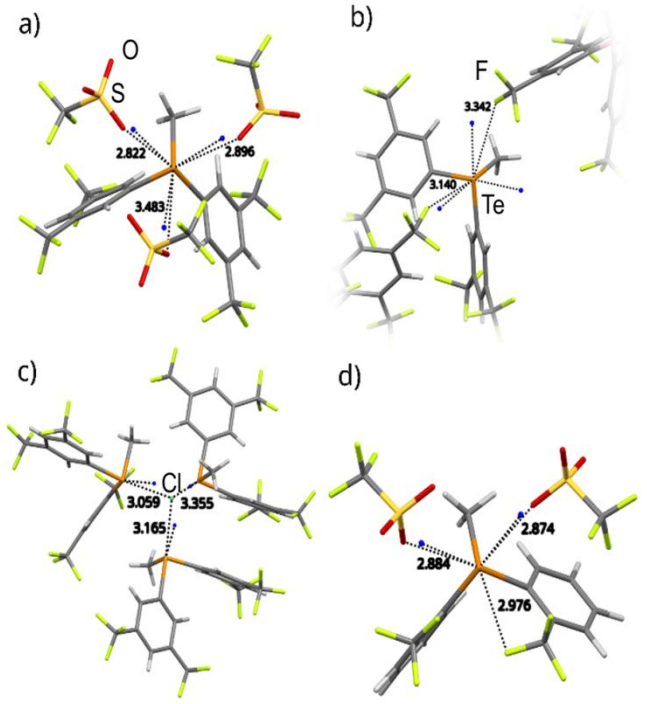

Figure 3. Selected X-ray Diffraction structures: a) **6a**, b) **6b**, c) **6e** and d) **7a**. Positions of σ_{ESP} are depicted by small blue spheres. Interatomic distances between Te (orange) and *A* = O (red), Cl (green), F (yellow green) atoms given in Å.

The σ_{ESP} positions (location of the σ-holes on the ESP surface) were superimposed for each crystal structure and compared with the position of the acceptor *A* atom (Figure 2 and Table S1 in ESI), the deviation between the two being calculated as the angle *α*(A-Te-σ_{ESP}). The average angular deviation 15.1(7.6)° revealed a good directionality of those σ-hole interactions based on the electrostatic property of the donor atom. Interestingly, this directionality is higher with *A* = O (α(A-Te-V_{max}) = 12.6(4.1)°) than with *A* = *F* (α(A-Te-V_{max}) = 19.7(11.7)°). This trend is correlated with the average *RR*, which is smaller for *A* = O than for *A* = F (respectively 0.83(4) and 0.89(5)). Comparatively, *A* = C_{Ar} are poor acceptors in this family with average *RR* = 1.04(8)

The telluronium cation **6**$^+$ was crystallized with six different mono anions (OTf^-, $BArF^-$, NO_3^-, Cl^-, SbF_6^-, ClO_4^-). With the $BArF^-$ anion (compound **6b**, Figure 3b), only two of the three Te σ-holes are clearly interacting with an acceptor (fluorine atoms of $BArF^-$), presumably due to the steric constrains imposed by the large anion and the poor acceptor properties of the latter. Similarly, in **3b** involving the same large anion, two of the three Te σ-holes are facing C_{Ar} placed at rather large distances with *RR* = 1.02/1.17. Those constrains may also be the reason why the most activated σ(Ar-Te) is in fact engaged in a longer interaction than σ(Me-Te) in this particular structure. On the contrary, in compound **6f** the smaller SbF_6^- anion leads to the occupation of the three Te σ-holes with fluorine atoms with a clear difference between σ(Me-Te) and σ(Ar-Te) (*RR* = 0.95 *vs*. 0.83) in line with the stronger activating power of -Ar fragment *vs*. -Me (131.2-135.8 kcal.mol^{-1} *vs*. 128.6 kcal.mol^{-1}). For **6**$^+$, the largest deviation of the position of the acceptor *A* atom with respect to the location of the σ-hole is observed in **6e** (average <*α*(*A*-Te-σ_{ESP})>=19.6(1.8)°). Indeed, in this compound the acceptor *A* = Cl is shared between σ-holes of three Te cations, inducing a balanced positioning of that atom (Figure 3c). On the contrary, *A* is closer to the Te σ-hole when *A* = O (especially OTf for which <*α*(*A*-Te-σ_{ESP})>=12.2(3.8)°): the extended structure of $-SO_3^-$ comparatively to Cl^- allows a better fitting to the electrophilic area of the Te cations (Figure 3a).

With -*R* = $-CH_3$, $-CF_3$ in *ortho* position to the Te-C_{Ar} bond (**7a-b**, **8a-b**), the telluronium cation adopts a conformation where the *R* groups are located in the area of the expected σ(Me-Te) hole, thus preventing intermolecular interaction in this direction. In these cases, the Te is shielded either sterically by the CH_3 group (**8a,b**) or electronically through ChB with a F atom from the CF_3 group (**7a,b**) (Figure 3d).

In summary, this structural study shows that up to three ChBs can be formed by the telluronium cations depending on the nature and position of the -*R* substituent on the -Ar group as well as on the nature and size of the counterion. Although these interactions are generally directional, the flexibility of the telluronium cations allows them to adapt their conformation to maximize the interaction with the counterion in the crystal state.

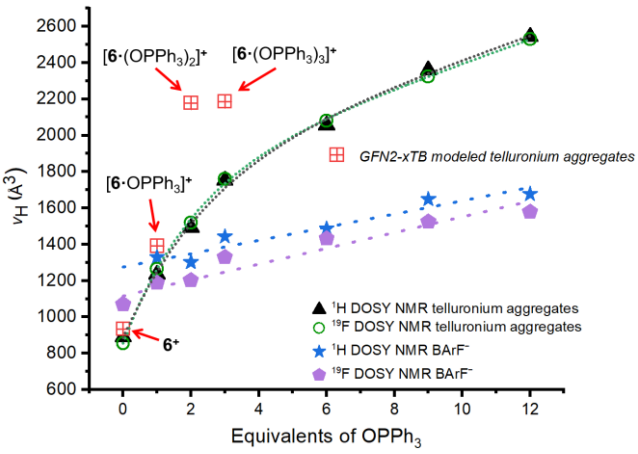

Figure 4. Evolution of the spherical hydrodynamic volume v_H of **6**$^+$ and $BArF^-$ upon addition of $OPPh_3$ to a solution of **6b** in CD_2Cl_2.

Diffusion-ordered NMR spectroscopy (DOSY) analysis of solutions of telluronium-Lewis base complexes

NMR monitoring of ChB in solution with tellurium-based derivatives can be performed by using triphenylphosphine oxide as Lewis base. [28, 60] Considering that each σ-hole of Te of the telluronium salts can interact with one phosphine oxide, three possible adducts are expected in solution: the mono-adduct [$Ar_2MeTe•OPPh_3$]$^+$, the bis-adduct [$Ar_2MeTe•(OPPh_3)_2$]$^+$ and the tris-adduct [$Ar_2MeTe•(OPPh_3)_3$]$^+$. To provide evidence for the formation of these adducts and to estimate their stoichiometry, ^{1}H DOSY measurements were performed on telluronium salts **6b-8b** with $BArF^-$ counterion in order to avoid as much as possible the anion/Lewis base competition (see ESI for details). First, the hydrodynamic diffusion coefficients *D* of the telluronium species formed upon incremental addition of $OPPh_3$ to telluronium **6b** were measured. For each considered **6b**:$OPPh_3$ ratio, a signal different from the one corresponding to the free telluronium was observed in the ^{1}H DOSY spectrum indicating

the presence of new species. The variation of *D* as a function of the stoichiometry of $OPPh_3$ is shown in Table S3 (cf. ESI), for which values of *D* were also determined by ^{19}F DOSY for cross-consistency: as the Lewis base is added the decrease in *D* damps starting from 3 equivalents of base and declines towards a limit value of *D* ~ 6.20 $10^{-10}m^2s^{-1}$ following an exponential decay. As *D* values of the cation tend to decrease, the value of *D* for $BArF^-$ also decreases to a lesser extent suggesting that as the cationic aggregate's volume is getting larger, its interaction with $BArF^-$ is becoming slightly tighter. This counter-intuitive fact may be rationalized by an increasing London-force-promoted ion pair aggregation and steric "attraction"[61-64] as the size of the cationic molecular complex increases.

To determine qualitatively the composition of the medium in 1:1, 1:2 and 1:3 complexes of salt **6b** with $OPPh_3$, *D* values were used to calculate the equivalent hydrodynamic volume v_H of the Te-centered cations and of the associated $BArF^-$ anion, assuming a spherical object model in the Stokes-Einstein theory[65, 66] (Figure 4).

In parallel, the geometries of ion pairs [**6**•$OPPh_3$][BArF], [**6**•$(OPPh_3)_2$][BArF] and [**6**•$(OPPh_3)_3$][BArF] were readily optimized using the Bannwarth-Ehlert-Grimme extended tight binding GFN2-xTB method[67, 68] with the Generalized Born model with Surface Area contributions (GBSA) for implicit solvation in dichloromethane (DCM), which allowed the generation of trial geometries of large sized salts at low computational cost (Table S5).

For the 1:1 and 1:2 complexes, the three combinations for the positions of $OPPh_3$ at Te were considered and the theoretical spherical hydrodynamic volumes v_{theo} (Figure 4, red squares) of the associated cations and $BArF^-$ were computed taking their largest dimension as the diameter of a rotating spherical object model, i.e. the largest interatomic distance (inter-hydrogen atoms) in the considered ion.

Comparison of the averages of v_{theo} with the experimental values of v_H suggests that at 1:3 ratio the presence in solution of [**6**•$OPPh_3$][BArF] and [**6**•$(OPPh_3)_2$][BArF] is tangible (Figure 4). At higher ratios the presence of [**6**•$(OPPh_3)_3$][BArF] is also tangible although a tighter binding of $BArF^-$ to this cationic aggregate may also be responsible for the larger v_H values. Therefore the presence in solution of the higher aggregate [**6**•$(OPPh_3)_3$][BArF] cannot be firmly ascertained. Note that control values of v_H extracted from ^{19}F DOSY experiments confirm the trend observed in ^1H DOSY for $BArF^-$ (Figure 4).

The ability of telluroniums **7b** and **8b** to form adducts with $OPPh_3$ was also investigated to check whether the shielding effect of the Te center observed in the solid state was maintained in solution. The diffusion coefficients and associated v_H measured after addition of 6 equivalents of $OPPh_3$ showed that in both cases the size of the formed species correlated well with a largely dominant 1:1 adduct (see ESI, Table S4). To further evaluate the maximum capability of the Te center of telluronium cations to bind Lewis bases in solution, isotherm calorimetric titrations were performed.

Isothermal titration calorimetry (ITC) of the association of telluronium salts with Lewis bases

In the present ITC[69, 70] study, we opted for the sequential addition of small volumes of a solution of Lewis base placed in the automated burette into a solution of the telluronium salt placed in the work cell at 25°C. 1,2-Dichloroethane (DCE) was used in all measures as the solvent owing to its low volatility (ITC jobs run for over 10 hours in an inert-gas filled glove box) and to the value of its dielectric constant (ε ~ 10.3) that is close to that of dichloromethane (ε ~ 8.9) used in DOSY-NMR experiments. In this setup, weak ionic strength changes induced by dilution were not considered.

The binding of a Lewis base (*B*) to a telluronium salt is expected to be directly influenced by the nature of the counterion and the ion pair existing in solution, that is either the solvent separated (2SIP), solvent shared (SIP) or contact (CIP) pair.[71] A solvated contact ion pair with possible pre-existing solvent-telluronium ChB in solution would make the interaction of a different Lewis base challenged by virtue of the law of mass action. Whether the ion pair type describing the telluronium salt in solution is "tight" (CIP) or "loose" (2SIP) is a lingering question that was only overflown in this study as shown above in the results of DOSY experiments, which outline the variation of the diffusion coefficient of the $BArF^-$ anion with the amount of added base.

In a first approximation, the telluronium–Lewis base association can be formulated (Chart 2) as a series of three equilibria wherein the Lewis base *B* potentially interacts with the three Te σ-holes. Whether this interaction is σ-hole selective[16] or not cannot be assessed experimentally but rather approached theoretically, as shown below. However, the three equilibria in (a)-(c) (Chart 2) can be used as a starting hypothesis to process ITC raw data. The feasibility of (b) and (c) (Chart 2) depends on the Lewis acidity and on the steric accessibility of remaining σ-holes at Te in both [Ar_2MeTe•*B*][X] and [Ar_2MeTe•$(B)_2$][X]. The binding of telluronium salts with Lewis base *B* is intuitively expected to follow this order: [Ar_2MeTe][X] > [Ar_2MeTe•*B*][X] > [Ar_2MeTe•$(B)_2$][X]. It may be anticipated that as the Te center is populated with *B*, the access to the remaining σ-holes becomes increasingly limited thus resulting presumably in lower equilibrium constants and less exothermic enthalpies of association.

$$[Ar_2MeTe][X] + B \overset{K_1}{\rightleftharpoons} [Ar_2MeTe{\bullet}B][X] \qquad \Delta H_1 \qquad (a)$$

$$[Ar_2MeTe{\bullet}B][X] + B \overset{K_2}{\rightleftharpoons} [Ar_2MeTe{\bullet}(B)_2][X] \qquad \Delta H_2 \qquad (b)$$

$$[Ar_2MeTe{\bullet}(B)_2][X] + B \overset{K_3}{\rightleftharpoons} [Ar_2MeTe{\bullet}(B)_3][X] \qquad \Delta H_3 \qquad (c)$$

Chart 2. The equilibria involved in the telluronium / Lewis base *B* association.

Prior analysis of raw heat flows

The thermograms shown in Figure 5 display typical responses of the telluronium $BArF^-$ salt **1b** and **6b** to the addition of volumes of a $OPPh_3$ solution in DCE (see Supp. Info. for the thermograms of various telluronium BArF salts). Since all ITC runs were carried out using identical concentrations of reagent and acquisition conditions, these figures are directly comparable and provide an intuitive insight into the strength of the exothermic response.

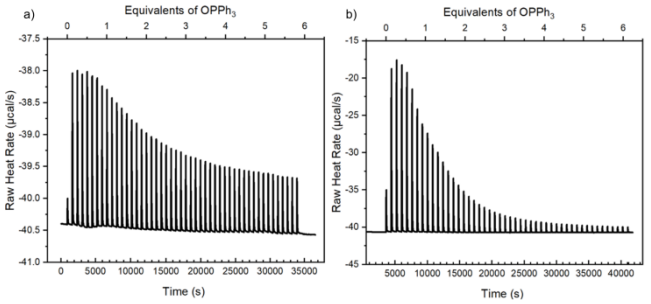

Figure 5. a) Example of weak *σ*-hole interaction: ITC thermogram of the interaction between **1b** and $OPPh_3$ in DCE. b) Example of strong *σ*-hole interaction: ITC thermogram of the interaction between **6b** and $OPPh_3$ in DCE. The processes are exothermic in all cases at 25°C and expressed in µcal/s versus time in s.

For instance, in Figure 5a (**1b** with $OPPh_3$) the maximum heat flow rate does not exceed 2.5 µcal/s whereas in Figure 5b (**6b** with $OPPh_3$) the heat flow culminates at a value higher than 16 µcal/s within the first 6 injections. The integration of heat flow peaks and the summation of these integrations up to the point of *relative athermicity*[≠] provides the raw heat Q_{tot} listed in Table 1 along with the related molar heats Q_{molar} for compounds **1b-8b**, where *N* is the stoichiometry in $OPPh_3$ at athermicity. Q_{molar} is determined here as the ratio Q_{tot}/number of moles of telluronium at *N* and thus can be assimilated to the "apparent enthalpy" of the equilibrated interaction between the telluronium salt and *N* equivalents of $OPPh_3$.

Table 1. Electronic effects of phenyl substituents on the raw and molar heats (Q_{tot} and Q_{molar}) of interaction between telluronium salts **1b**-**8b** and $OPPh_3$ in DCE.[a]

[Ar_2MeTe] [BArF$^-$] (-R)	Q_{tot}[b] (µcal)	Q_{molar}[c] (kcal.mol^{-1})	N[d]	σ_m[e]
1b (-3,5-*t*Bu)	-420 ± 9	-0.127 ± 0.006	3.9	-0.1
2b (-H)	-794 ± 2	-0.369 ± 0.001	3.6	0
3b (-3,5-OMe)	-894 ± 40	-0.41 ± 0.02	4.1	+0.12
4b (-3,5-C≡C-*n*Pr)	-1790 ± 169	-0.82 ± 0.08	3.6	+0.21[f]
5b (-3,5-Cl)	-2202 ± 130	-1.00 ± 0.06	3.9	+0.37
6b (-3,5-CF_3)	-2504 ± 53	-1.14 ± 0.02	3.8	+0.43
7b (-*o*-CF_3)	-1774 ± 122	-0.81 ± 0.06	3.4	-
8b (-*o*-CH_3)	-575 ± 4	-0.261 ± 0.002	3.9	-

[a] Conditions: sample cell (telluronium salt), *c* = 2.0 mM; syringe ($OPPh_3$), *c* = 131.1 mM. The titrations were performed at 25°C through 48 sequential additions (of 2.06 µL each), time delay between two consecutive injections was 800 s. [b] Total energy released corrected by dilution term. [c] Molar enthalpy obtained by dividing Q_{tot} by the molar quantity of telluronium. [d] Number of equivalents of $OPPh_3$ needed to achieve athermicity. [e] Empirical σ_m parameters for aryl substituents in *meta* position[72]. [f] The σ_m for -C≡C-*n*Pr was assimilated to that of -C≡C-Me.[72]

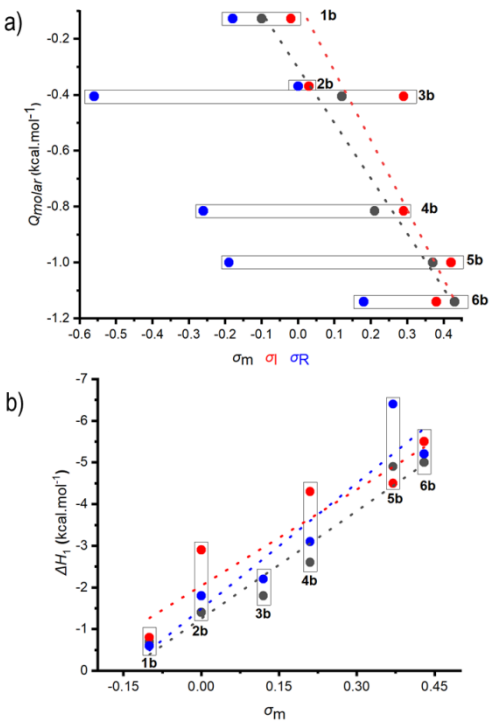

Figure 6. a) Plots of the molar heat of association Q_{molar} (kcal/mol) in DCE at 25°C *vs* σ_m (R^2= 0.95) , σ_I (R^2= 0.71) and σ_R parameters.[72] b) Plots of ITC-derived values of ΔH_1 for the 1:1 interaction of **1-6b** with $OPPh_3$ in DCE *vs* σ_m from the considered thermodynamic models **3S** (R^2 = 0.94, grey dots), **2S** (R^2 = 0.82, red dots), **IM** (R^2 =0.87, blue dots) at 25°C.

Q_{molar} somewhat represents a convoluted combination of the intrinsic enthalpies of equilibria in equations (a)-(c) (Chart 2) that translates the structural differences existing between the considered telluronium salts into sensible variations of heat release. The first feature that emerges from Q_{molar} values is the influence of the electronic effect of the substituents at the phenyl groups; the higher the electron-withdrawing effect the more exothermic the values of Q_{molar}. The Hammett plots[72] of both Q_{tot} and Q_{molar} drawn for telluroniums of the same class, all containing *meta* disubstituted phenyl groups, i.e **1-6b**, show a clear linear correlation with σ_m values, whilst the *N* values all sit in the 3.6 – 4.1 eq. range, or in other terms at an average value of ~(3.9 ± 0.3) eq. (Figure 6a and ESI). Interestingly, a linear correlation is found with the inductive effect-related σ_I parameter whereas no correlation exists with the resonance parameter σ_R, which suggests that the Lewis acidity at Te is mainly governed by inductive electronic effects that are transferred by the cation's backbone.

For salts **7b** and **8b**, Q_{molar} values are directly impacted by electronic effects, although the foreseen partial occlusion caused by the *ortho* substituents could be responsible for the values of Q_{molar}(**7b**) and Q_{molar}(**8b**).

Q_{molar} depends also on the counterion's unpairing energy payload that has to be overcome to allow any Lewis base to bind the Te center. For **1-8b**, the BArF$^-$ anion that is known to have a low coordinative ability due to the large delocalization of charge density on peripheral F atoms seemingly exclude a strong binding interaction with the Te center. The influence of the counterion's nature on the apparent enthalpy of association Q_{molar} for an interaction with $OPPh_3$ was evaluated with BArF$^-$

(**6b**), BF_4^- (**6c**), Cl^- (**6e**), $[B(C_6F_5)_4]^-$ (**6g**) and ClO_4^- (**6h**) (cf ESI, Figure S5a). A tentative rationalization of these results was performed by comparing the values of Q_{molar} in each case to the a_{TM} parameter proposed originally by Alvarez et *al.*[73] in 2011 and updated in 2020[74] to characterize the affinity of anions to transition metal-centered cations. However, the data (Figure S5a) indicated that the values of Q_{molar} do not correlate with a_{TM}.

The propensity of several Lewis bases to interact with **6b** (Table 2) was also evaluated. Worthy to note, a slow decomposition of the telluronium cation occurred with strong Lewis bases such as PPh_3, quinuclidine and DBU (1,8-diazabicyclo[5.4.0]undec-7-ene). In each case, the formation of a low amount of the parent diaryltellane was observed by ^1H NMR as a result of nucleophilic methyl transfer to the base (see ESI). Moreover, precipitate formation was observed with these bases probably arising from the nucleophilic substitution of the DCE solvent.[75] These reactions precluded any further ITC experiments: indeed, the extent of the contamination by spurious heat flow arising from the nucleophilic substitution reactions was difficult to evaluate.

Table 2. Thermochemical data of the titration of **6b** with various Lewis bases in DCE.[a]

entry	Lewis base	Q_{tot} (µcal)	Q_{molar} (kcal.mol^{-1})	*N*
1	$OPPh_3$	-2156 ± 94	-0.97 ± 0.04	3.8
2	$OPEt_3$	-2540 ± 17	-1.183 ± 0.008	3.9
3	PyrNO	-1518 ± 213	-0.7 ± 0.1	3.9
4	DMSO	-1260 ± 55	-0.57 ± 0.03	3.1
5	TBACl	-3426 ± 127[b]	-1.56 ± 0.06	2.5

[a] Conditions: see Table 1. [b] value most probably contaminated by side demethylation reaction.

In the case of tetra(*n*-butyl)ammonium chloride (TBACl) though, only the demethylation reaction was observed, which consumed a little less than 10% of **6b**. Therefore, the value given in Table 2 (entry 5) seems contaminated by an exothermic contribution arising from telluronium's demethylation reaction.
Neutral organic oxides, namely $OPEt_3$, PyrNO (pyridine *N*-oxide) and DMSO (dimethylsulfoxide) were found inactive in the demethylation side reaction and provided neat exothermic responses when injected into a solution of **6b** (Table 2).

Enthalpies and association constants from deconvoluted ITC thermograms.

The main application of ITC is the determination of thermodynamic parameters of ligand-host interactions. Most of the numerical methods developed so far in the domain of biophysics[76, 77] focus on providing access to significant thermodynamic parameters of the interaction of biologically relevant hosts (peptides and enzymes) with various guests. In this study, three different thermodynamic models of chemical associations that use recursive multi-parametric refinement and curve fitting algorithms were applied and compared based on the information provided experimentally by DOSY-NMR.

Those models are the following: the Sequential Three-Site Binding Model[78] (noted **3S**), the Sequential Two-Site Binding Model[79, 80] (noted **2S**) and the (one site) Independent Model[81] (noted **IM**). The latter was particularly instrumental with **7b** and **8b** in determining a plausible enthalpy of interaction for telluronium cations that would a priori hardly bind readily two bases due to the cluttering at the Te center that is caused by the *ortho* methyl and trifluoromethyl groups of the aryl moieties.

Table 3. Thermodynamic parameters (enthalpies and association constants) for the interaction of telluronium BArF salts **1b**-**8b** with $OPPh_3$ in DCE at 25°C as inferred on the basis of models **2S** and **IM**.[a]

	Model **2S**			
salt	$\Delta H_1^{b,c}$	$\Delta H_2^{b,c}$	K_{a1}^{c}	K_{a2}^{c}
1b	-0.8 ± 0.1	+0.7 ± 1.1	(2.9 ± 1.2)10^3	(2.8 ± 3.1)10^2
2b	-2.9 ± 0.1	+4.6 ± 2.5	(6.4 ± 0.6)10^2	10 ± 6
3b	-2.2 ± 0.1	+1.3 ± 0.7	(1.1 ± 0.1)10^3	10 ± 3
4b	-4.3 ± 0.1	+2.3 ± 0.8	(1.3 ± 0.1)10^3	10 ± 3
5b	-4.5 ± 0.1	-1.9 ± 0.2	(5.6 ± 0.4)10^3	(1.3 ± 0.1)10^2
6b	-5.5 ± 0.1	-1.4 ± 0.1	(6.9 ± 1.0)10^3	(8.9 ± 0.6)10^2
7b	-3.8 ± 0.1	-0.5 ± 0.1	(2.0 ± 0.4)10^4	(4.5 ± 1.3)10^2
8b	-1.8 ± 0.4	+1.4 ± 1.7	(5.1 ± 2.1)10^2	(2.1 ± 3.1)10^2
	Model **IM**			
	$\Delta H^{[a]}$	*n* ($OPPh_3$)	K_a^{a}	
1b	-0.6 ± 0.2	1.3 ± 0.2	(1.0 ± 0.3)10^3	
2b	-1.8 ± 0.1	1.3 ± 0.06	(1.3 ± 0.1)10^3	
3b	-2.2 ± 0.1	0.97 ± 0.05	(1.1 ± 0.1)10^3	
4b	-3.1 ± 0.1	1.22 ± 0.02	(2.2 ± 0.1)10^3	
5b	-6.4 ± 0.2	0.85 ± 0.02	(1.8 ± 0.06)10^3	
6b	-5.2 ± 0.1	1.19 ± 0.01	(2.6 ± 0.07)10^3	
7b	-4.2 ± 0.1	1.01 ± 0.01	(6.4 ± 0.2)10^3	
8b	-0.9 ± 0.1	1.51 ± 0.10	(10.0 ± 1.6)10^2	

[a] cf. ESI for the full table including model **3S**. [b] enthalpies are expressed in kcal.mol^{-1}. [c] standard errors from replicate determinations.

Table 3 provides a concise list of the main thermodynamic parameters inferred from models **2S** and **IM**; note that Table S6 (see ESI) lists the full thermodynamic parameters produced by all the considered models from ITC thermograms collected for the titrations of **1b-8b** with $OPPh_3$. In the latter table, it can be noticed that the greatest standard errors that can climb over 100% are on association constants calculated with **3S**. The enthalpies are much less affected and errors are held lower than 10%. The values of enthalpies suggest a decrease of exothermicity as the Te center is populated with Lewis bases.
The marked endothermicity of ΔH_3 justified that the third binding equilibrium in (c) (Chart 2) be neglected, leading thus to the evaluation of the **2S** model. By resorting to this model, the errors on equilibrium constants were greatly reduced. Also worthy of note, the absolute values of association enthalpies

only slightly increased. Overall, the **2S** model produced smoother convergence of data fitting.

The **IM**, which suits a model of predominant 1:1 interactions, gives consistent values in the case of **7b**. The same is not true with **8b**, for which refinement of the *n* index of stoichiometry repeatedly pointed to a value of 1.5, suggesting the possibility of the existence in solution of the [**8b**•$(OPPh_3)_2$] complex, which is consistent with the ESP analysis. The use of **IM** for all the other cases, *i.e.* for **1b-6b** does not provide realistic stoichiometry factors and produces much lower values of association constants, although with lower standard errors than models **3S** and **2S**. Nonetheless, the use of **IM** in parallel with **2S** provides a reliable estimation of the range of values for the first association constant for sterically encumbered Te centers in **7b** and **8b**.

It is worthy to note that the best fit for both ΔH_1 and ΔH_2 is for the interactions between **3b-6b** and $OPPh_3$ with errors lower than 20% of the nominal value of enthalpy. There is no other criterion for evaluating the most suitable model producing reliable association constants than gauging the errors generated by each thermodynamic model. As a matter of fact, much lower errors on ΔH_1 are found with **2S** and **IM**. Note that Tables S7 and S8 (see ESI) provide a similar list of thermodynamic parameters produced by the three considered models for the base affinity study (Table S6) and the counterion influence (Table S8, ESI).

The lowest errors on the first association constant K_{a1} are obtained with model **2S**, while the error and value differentiation for ΔH_1 and ΔH_2 on going from $OPPh_3$ to DMSO in Table S7 or from **6b** to **6e** in Table S7 between **3S** and **2S** models are relatively invariable. The results listed in Tables S6-S8 (ESI) provide rather consistent substituent-dependent and steric cluttering–dependent trends for the interaction of telluroniums **1b-8b** with oxygen-based Lewis acids and particularly with $OPPh_3$ in a DCE solution.

Figure 6b gathers the values of ΔH_1 determined by the three considered models. It shows a satisfactory correlation with σ_m allowing to estimate the enthalpy of formation of a 1:1 complex in DCE for any [Ar_2MeTe][BArF] salt containing identical *meta* substituents at the two Ar groups. For instance, a linear fitting (R^2= 0.86) carried out with all the points of the curve in Figure 6b provides the following equation that allows to predict the ΔH_1 value expected for {[3,5-$(X)_2C_6H_3$]$_2$MeTe}[BArF] in DCE:

$$\Delta H_1 = (-1.5 \pm 0.2) + (-8.7 \pm 0.8) \times \sigma_m \text{ (in kcal/mol)}$$

While the determination of Q_{molar} provides an unbiased measure of the exothermicity of the interaction of a Te center with a Lewis base, the deconvolution of thermograms disclosed here with algorithms defined for specific thermodynamic models require careful critical inspection of the statistical errors on the inferred thermodynamic parameters.

It can safely be stated nonetheless that ΔH_1 in the BArF salt series varies from ca. -0.5 to -5.0 kcal/mol on passing from double *meta*- electron-donating to electron-withdrawing substitutions at the Te-borne phenyl groups. Caution seems warranted on the values of ΔH_2 though; only those enthalpies related to **6b** in its interaction with $OPPh_3$ are reliable.

The complementarity of ITC with DOSY experiments is compelling: ITC provides a rather reliable assessment of the predominant formation of 1:1 complexes of telluronium cations with Lewis bases in all the cases where the aryl groups are *meta*-disubstituted.

Bonding and *in solutio* thermochemistry of the telluronium-base interactions.

The binding interaction between a rather weak Lewis base ($OPPh_3$) and the [$Ar_2MeTe]^+$ cation is reminiscent of that encountered in conventional weak Lewis pairs where the binding centers are engaged in a weak dative bond (covalent or shared) or in so-called "frustrated" pairs.[82] Several reports have already outlined the origin of the cohesion of unusual solution (and solid-state)-persistent[83] "Lewis pairs" that cannot solely stem from a frail covalent bond between two atomic centers.[84] The view of an "all driving dative (covalent) bond" is outdated and applies only to a part of Lewis-pairs. It was already shown that cohesion often stems from the combination of a weak covalent bonding (orbital interaction-based charge density transfer officiating as a local anchoring point for two molecular fragments) with a predominant stabilization by London force (also known as dispersion force) [85, 86] acting remotely between the groups (or ligands) of the donor-acceptor pair.[84] In a number or cases molecular complexes (dimers, oligomers) do not even possess a local covalent intermolecular anchoring component[87] and may be even persistent in solution.[88]

A model of the ChB-based molecular complexes studied here was analyzed from both the local and non-local viewpoints by accounting for the role of the surrounding substituents and their mutual interaction so as to identify the "forces" that drive and govern the association depicted as being centrally a ChB.

At the local level, a range of complementary analytical tools were used jointly with the DFT (density functional theory); these are EDA (energy decomposition analysis),[89] ETS-NOCV (extended transition state-natural orbital for chemical valence)[90], QTAIM (quantum theory of atoms in molecule)[91, 92],¶, IQA (interacting quantum atoms)[93-95],¶, NCIplot[96], IGM (independent gradient model)[97] and the associated IBSI (instrinsic bond strength index)[98],‡, which are particularly adapted to the analysis of short-range interatomic interactions.

For the analysis and decomposition of non-local interactions acting between bonded fragments, the use of the LED (local energy decomposition)[99] at the DLPNO-CCSD(T)[100],∂ (domain-based local pair natural orbital coupled cluster theory with single, double, and perturbative triple excitations) level of theory was preferred.

Optimized geometries and densities serving the above mentioned analyses were computed at the ZORA (zeroth order relativistic approximation)[101]-PBE[102]-D4(EEQ[54])/all electron TZP /COSMO[103](DCE) level of theory used here as a standard method. It must be noted that the impact of the type of dispersion correction on computed observables is one significant issue that is also addressed in the section dealing with the thermochemistry of the telluronium-$OPPh_3$ association.

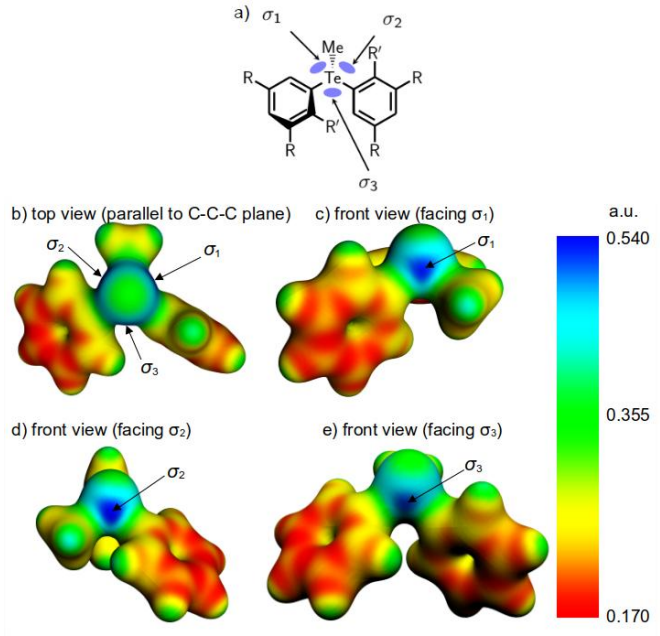

Figure 7. a) numbering and position of the σ-holes $\sigma_{1\text{-}3}$ in $[Ar_2MeTe]^+$. b-e) different views of the DFT-determined electrostatic potential map for $\mathbf{2}^+$ drawn on an isosurface of the density (0.03 $Å^{-3}$) showing the localisation of $\sigma_{1\text{-}3}$.

Table 4. V_{max} values (in kcal/mol) calculated for the 1:1 and 1:2 adducts of $\mathbf{2}^+$ with $OPPh_3$ facing different σ-holes.

site(s) for $OPPh_3$ binding	$V_{max,\sigma1}$ [a]	$V_{max,\sigma2}$ [a]	$V_{max,\sigma3}$ [a]
$\mathbf{2}^+$			
none	119.5	117.2	108.0
$[\mathbf{2}\bullet OPPh_3]^+$			
σ_1	-	102.2	92.7
σ_2	104.7	-	95.9
σ_3	104.5	99.4	-
$[\mathbf{2}\bullet(OPPh_3)_2]^+$			
$\sigma_{1,2}$	-	-	74.5
$\sigma_{1,3}$	-	83.5	-
$\sigma_{2,3}$	83.7	-	-

[a]computed from the optimized geometries at the ZORA-PBE-D4(EEQ)/(all electron)TZP/COSMO(DCE) level of theory.

Properties of telluroniums' σ-holes and their interaction with $OPPh_3$.

In a static representation of the telluronium cation, the three σ-holes are inequivalent, as the two aryl groups have different orientations; one is almost orthogonal to its C_{Me}-Te-C_{Ar} plane, position σ_1, the other is almost coplanar to its C_{Me}-Te-C_{Ar} plane, position σ_2 (Figure 7). However, the two aryl groups rotate rather freely around their respective Te-C_{Ar} axes nearly barrierless ($\Delta G^{\ddagger}$ < 1 kcal/mol for $\mathbf{2}^+$ at the ZORA-PBE-D4(EEQ)/(all electron)TZP/COSMO(DCE) level of theory). The values of the maxima of the electrostatic potential surface (V_{max}) corresponding to the three σ-hole sites are detailed in Table 4 (see also Table S15 in ESI).

The influence of a Te(IV)-bound Lewis base on the values of the V_{max} of the remaining vacant σ-holes was investigated with the possible 1:1 and 1:2 complexes derived from $\mathbf{2}^+$ with one or two molecule(s) of $OPPh_3$ binding the Te center, considering combinations with the three possible positions of occupation (Table 4).

Regardless of the σ-hole(s) occupied by $OPPh_3$ in the 1:1 and 1:2 adducts considered here, it is found that the V_{max} potential of any unoccupied σ-hole decreases linearly with the occupation of the other sites: the association of one base with one σ-hole decreases the V_{max} potential of the two others by *ca*. 21 kcal/mol, and the association of a second base again decreases the V_{max} potential of the remaining free σ-hole by another 21 kcal/mol. Noteworthy, the plot of the Hammett σ_m parameters[72] with the V_{max} values of the σ-holes of Te in di(3,5-disubstituted-aryl)methyltelluroniums ($\mathbf{1}^+$-$\mathbf{6}^+$) (Fig. S9, ESI) shows a non-linear scattered correlation[16, 104, 105]; the V_{max} potential values of the three σ-holes growing with Hammett–Taft's[72] σ_m values.

The $[Ph_3PO\bullet TeAr_2Me]^+$ interaction: a weak donor-acceptor bond with a dominant attractive Coulombic interaction.

The easiest way to assess the donor-acceptor (Lewis) character of a molecular complex is by evaluating the charge transfer occurring upon formation of the Lewis pair. This can be done readily by computing the sum of atomic Bader charges[106] Σ*q*(donor) and Σ*q*(acceptor) on each fragment of the pair. In the following, only one structural type of telluronium-$OPPh_3$ pair among the three possible combinations shown above was chosen.

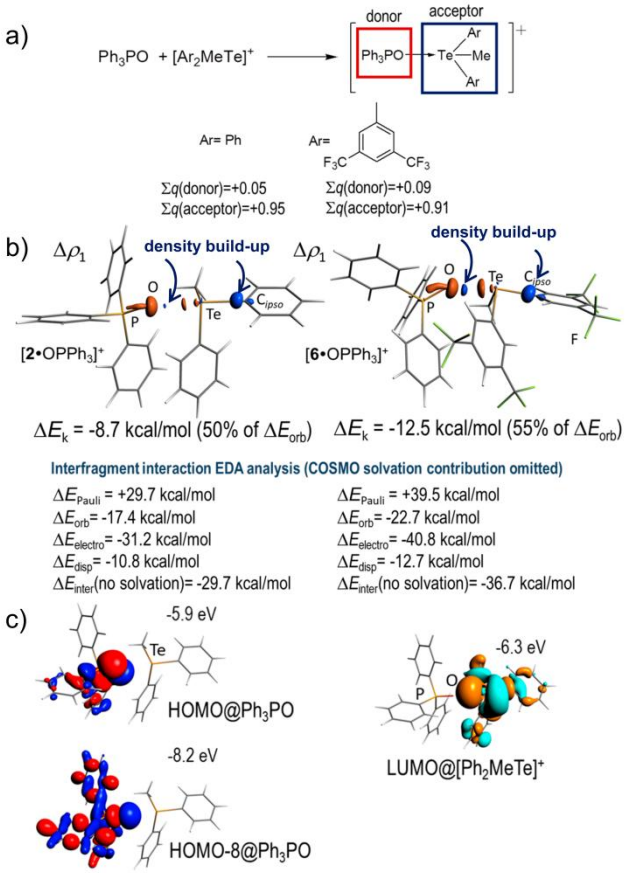

Figure 8. a) Analysis of the distribution of Bader charges[91] in [**2**•OPPh$_3$]$^+$ and [**6**•OPPh$_3$]$^+$: significant charge density transfers from the Lewis donor OPPh$_3$ to the acceptor [Ar$_2$MeTe]$^+$ resulting in a partially positively charged donor in the adducts. b) ETS-NOCV deformation density isosurface plots (0.005 Å^{-3}) for the strongest inter-fragment NOCV interactions $\Delta\rho_1$ in [**2**•OPPh$_3$]$^+$ and [**6**•OPPh$_3$]$^+$ and associated EDA. c) SFOs involved in the build-up of $\Delta\rho_1$ in [**2**•OPPh$_3$]$^+$.

Similar conclusions can be drawn for the two other types of pairs. In the case of **2**$^+$ and **6**$^+$ the analysis of Σq indicates that a significant charge density transfer occurs in both cases from OPPh$_3$ (the Lewis donor) to the [Ar$_2$MeTe] (the Lewis acceptor) fragment; the positive value of Σq(OPPh$_3$) being larger when the acceptor is the electron-withdrawing CF$_3$-substituted **6**$^+$ (Figure 8a).

The IQA[93] provides another compelling quantification of the O-Te interaction in [**2**•OPPh$_3$]$^+$ in terms of Coulombic and covalent character (E_{inter}(O-Te)= -266 kcal/mol, $E_{covalent}$(O-Te)= -23.3 kcal/mol and $E_{coulombic}$(O-Te)= -243.6 kcal/mol) and [**6**•OPPh$_3$]$^+$ (E_{inter}(O-Te)= -298.3 kcal/mol, $E_{covalent}$(O-Te)= -28.6 kcal/mol and $E_{coulombic}$(O-Te)= -269.7 kcal/mol). The obtained values show that it is by ~90 % and ~10% attractively coulombic and covalent in character respectively in both cases.

Therefore, most of the charge density transfer occurs via a minute channel of covalent (shared) interaction that can be readily analyzed by the ETS-NOCV method[90] considering the molecular fragmentation scheme for a dative O→Te bond.[107] Figure 8b depicts the amplitude of the charge density transfer upon interaction of the two considered fragments by way of the isosurfaces of the deformation density where red isosurfaces correspond to depleted density volumes and blue ones to those enriched by the interaction between the two molecular fragments. The major part of the density is transferred to the *ipso* aromatic Te-bound carbon (C_{ipso}, Figure 8b) and a minor part builds the frail covalent component of the O-Te interaction.

In the case shown here one can consider the highest value of ΔE_k for [**6**•OPPh$_3$]$^+$ as compared to [**2**•OPPh$_3$]$^+$ as a direct consequence of the electron-withdrawing effect operated by the four -CF$_3$ groups, which tends to slightly consolidate the covalent character of the O-Te interaction. The analysis of the symmetry combination of fragment orbitals (SFOs) giving rise to $\Delta\rho_1$ reveals the latter's origin in the interaction of two occupied orbitals of the OPPh$_3$ fragment, i.e. the HOMO and the HOMO-8, with the LUMO of the [Ar$_2$MeTe]$^+$ fragment, which contains a rather important lobe at Te pointing towards the O atom (Figure 8c). Scrutiny of the geometry confirms that the O-Te interaction impacts Te-C$_{Ar}$ bond *trans* to it, making it slightly longer by ~0.03 Å than that of Te-C$_{Ar}$ bond associated with the aromatic ring *cis* to the O donor.

The QTAIM analyses of [**2**•OPPh$_3$]$^+$ and [**6**•OPPh$_3$]$^+$ suggest the existence of a bond path and bond critical point (BCP (3,-1)) in the O-Te segment with an electron density at the BCP of *ca.* 25-30% that encountered for the BCPs of typical covalent single Te-C bonds in the same molecule. In turn, the ADF-NCIPlot[96] analysis points to a dominant attractive O-Te noncovalent interaction (NCI), which is confirmed by the IGM$^{\#}$,[97, 108]-IBSI‡,[98] values that are all within the range proposed by Hénon *et al.* for NCI[98] (cf. ESI, Table S16). A qualitative graphical analysis of these systems (cf. ESI, Figures S10) shows that the main attractive feature is located between the Te and the O (blue isosurfaces). However, different non-bonding features (green isosurfaces) of variable extent appear between different regions of the two fragments and are assigned to weak hydrogen bonds or CH-π interactions.

Also, non-bonding features mainly appear between the O and nearby hydrogens of the telluronium fragment, which might be viewed as weak H-bonds, thus stressing that the cohesion of the adduct does not solely stem from the O-Te ChB. The general tendency of the O-Te IBSI values is towards a non-monotonous increase of the interaction as the electron-withdrawing character of the substituent grows from a value of 0.062 ([**1**•OPPh$_3$]$^+$) to a value of 0.089 ([**6**•OPPh$_3$]$^+$) (see ESI Table S19).

Within the IGM scheme, atomic contributions to the inter-fragment interaction were determined to outline the relative participation of each atom to the overall inter-fragment interaction.[97] An atomic decomposition of the interaction between telluroniums **1**$^+$-**6**$^+$ and a OPPh$_3$ molecule, be it in a 1:1, 1:2 or 1:3 adduct (see ESI, Tables S18 and S19), confirms that the atoms contributing the most to this interaction are Te and O. However, they each only contribute to between 5 and 25% of the overall telluronium-OPPh$_3$ interaction, thus evidencing that the cohesion of the adduct cannot be reduced solely to the two atoms involved in the ChB.

Studies carried out at the non-local level further confirm the drive of electrostatics supported by London's dispersion in the self-aggregation of telluronium cations and OPPh$_3$ in the gas phase.

Non-local interactions from LED / DLPNO-CCSD(T) analysis.

The analysis of non-local interactions supporting the formation of a molecular complex from two or more fragments

requires the physically sound decomposition of an inter-fragment interaction energy term into meaningful canonical interactions.

Compared to DFT-D methods that consist of native DFT functionals patched with a correction term accounting for dispersion / van der Waals interactions, wavefunction theory (WFT)-based methods give access to physically consistent energy decompositions and quantifications of noncovalent contributions. [109-111]

By the use of adequate energy decomposition schemes, the mapping of the interactions acting in the periphery of the main fragment-anchoring interaction is possible and allows the evaluation of the importance of NCIs in the process of molecular aggregation. [85, 88]

Neese and Bistoni outlined the analytical power of the LED[99] / DLPNO-CCSD(T)[100, 112, 113] method∂ which was used to trace down the importance of dispersion in the structuration of agostic C-H…metal interactions. The DLPNO-CCSD(T) method combines the high-accuracy of the coupled-cluster approach with the reduced computational cost[114] stemming from the localisation of the orbitals constructed at the Hartree-Fock level. The LED[99] analysis∂ allows the extraction of the various contributions of user-defined interfragment interactions in a way reminiscent of the EDA[115] as applied to DFT calculations.

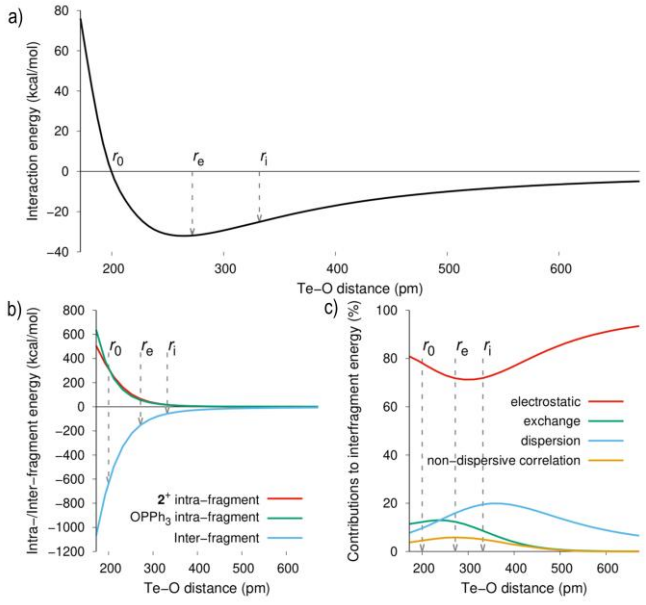

Figure 9. a) Interaction energy curve for the $[\mathbf{2}\bullet OPPh_3]^+$ adduct along the O-Te distance at the DLPNO-CCSD(T)/def2-TZVP level of theory. b) Plot of the intra- and inter-fragment energies. c) The contributions to the inter-fragment energy with the localisation of remarkable O-Te distances r_i, r_e and r_0.

The LED[99]/DLPNO-CCSD(T)[100, 112, 113] analysis was therefore applied to $[\mathbf{2}\bullet OPPh_3]^+$ in its ZORA-PBE-D4(EEQ)/all electron TZP/COSMO(DCE)-optimized geometry wherein $OPPh_3$ faces the σ-hole σ_2 (see Figure 8): $\mathbf{2}^+$ being the first fragment and $OPPh_3$ the second one. The analysis was carried out in the gas phase by varying the O-Te distance keeping fragments' geometries rigid.

This approach, although rather simplified, provides a good picture of the interactions that play a significant role in the formation of the molecular complex (Figure 9). The validity of the chosen fragmentation used in the LED[99] analysis was verified by the analysis of the Mülliken population showing that none of the localized molecular orbitals are delocalized on both fragments for O-Te distances above 152 pm. This also confirmed that the fragments are not strongly covalently bonded even at such O-Te distances shorter than the equilibrium distance r_e (Figure 9).

Within the chosen fragmentation scheme, on moving from a long distance to r_0= *d*(O-Te) = 200 pm, the stabilizing inter-fragment contribution surpasses the sum of the intra-fragment ones. At distances longer than *ca*. 200 pm, even if both fragments are partly individually destabilized in the presence of the other, their mutual interaction nonetheless favors the formation of the adduct through an overly stabilizing inter-fragment energy term. Considering both intra-fragment contributions, the $OPPh_3$ fragment is more destabilized than $\mathbf{2}^+$, except around the equilibrium O-Te distance r_e (r_e= *d*(O-Te) = 292 pm) (Figure 9b). The stabilizing electrostatic contribution, dominated by electron-nucleus attraction energy terms, represents more than 72% of the inter-fragment energy at any O-Te distance (Figure 9c) with a minimum close to r_e. In turn, the exchange contribution accounts for less than 13% of the inter-fragment energy, with a maximum around r_e. The dispersion force contribution surpasses the exchange one at distances longer than r_e, reaching apex with 17% of the inter-fragment energy around the inflection point distance r_i (r_i = *d*(O-Te) = 332pm) of the interaction energy curve.

Table 5. Computed enthalpies and Gibbs free energies of association of one $OPPh_3$ with diarylmethyltelluroniums ($\mathbf{1}^+$-$\mathbf{6}^+$) at position σ_2.

telluronium cation	ΔH_1 (kcal/mol) [a]	ΔG_1 (kcal/mol) [a]
$\mathbf{1}^+$ (-R= -*t*Bu)	-12	+2
$\mathbf{2}^+$ (-R = -H)	-11	+3
$\mathbf{3}^+$ (-R= -OMe)	-11	-1
$\mathbf{4}^+$ (-R= -C≡C-*n*Pr)	-13	0
$\mathbf{5}^+$ (-R = -Cl)	-14	0
$\mathbf{6}^+$ (-R= -CF_3)	-20	-9

[a] at 298.15 K, ZORA-PBE-D4(EEQ)/all electron TZP/COSMO(DCE).

These results demonstrate that the ChB between $\mathbf{2}^+$ and $OPPh_3$ is overwhelmingly non-locally noncovalent in nature and only weakly covalent at a local level as the system reaches r_e. From r_e to shorter distances exchange becomes effective and acts as an evanescent intermolecular anchor that opens a narrow channel for charge density transfer.

Influence of solvation and of the pair-wise *vs*. many-body DFT dispersion / van der Waals corrections on the thermodynamics of association.

In solution, solvent screening, ion pairing and possible explicit interactions of solvent molecules may temper the attractive electrostatic interactions existing between the telluronium cation and a neutral Lewis base by screening. Dispersion force though might well also be compensated[116] but this issue is still not fully

settled.[117] The complex problem of solvation was not addressed thoroughly here but, owing to the size of the molecular objects, merely approached from the viewpoint of thermodynamics by using static DFT-D methods and comparing implicit and explicit solvation schemes with two differently constructed dispersion/van der Waals-corrected functionals, that is the pair-wise –D4[54] corrected PBE[102] and the many-body –MBD[56] corrected PBE (see next section) in the static DFT regime.

As shown in the previous section with the DLPNO-CCD(T) investigation on a rigid model, dispersion force plays a supportive role in the cohesion of telluronium-$OPPh_3$ complexes; the scrutiny of the quality of the scaling of various the dispersion corrections provided for large molecular complexes at the DFT level is therefore justified(*vide infra*).

Also important to stress is that the thermodynamics of the first association of $OPPh_3$ with telluroniums (**1**$^+$-**6**$^+$) on position σ_2 computed at the ZORA-PBE-D4(EEQ) using only implicit solvation (Table 5) diverge significantly from the best experimental values provided by ITC experiments and the associated thermogram deconvolutions (Table 3).

This is not surprising, though. There exist occurrences of good match between COSMO[103] (or other continuous screening solvation models)/ DFT-D computed thermochemistry parameters with ITC data for systems implying neutral molecules (or bearing highly delocalized charges).[118-121] However, significant discrepancies have been often reported for chemical reactions involving salts,[122, 123] in which the counter ion is systematically omitted in DFT calculations and the solvent happens to be a discrete actor. The question of solvation addressed using COSMO[103] either fully implicitly or with explicit amount of solvent applied to isolated ions may reputedly produce inaccurate solvation energy contributions.[124] Added to this are the inaccuracies inherent to the rigid rotor harmonic oscillator approximation that question the reliability of computed enthalpies and Gibbs free energies of weakly bonded molecular complexes, for which critical intermolecular vibrational modes in van der Waals complexes show up at low frequencies in the ~0-200 cm^{-1} region. [125-127]

The plot of the computed Gibbs free energies of association *vs*. σ_m parameters and the enthalpies (Table 5) tells that the association is increasingly exergonic as the value of the σ_m parameter grows from electron-donating substituents to electron-withdrawing ones. This is the only conclusion of static DFT computations that converges with ITC results. Such a result provides nonetheless worthy information on the role of solvation and its tendency to damp the absolute values of enthalpies of association as compared to gas phase calculated values (*vide infra*).

Here, the thermodynamics of association of one or two molecules of $OPPh_3$ with **2**$^+$ were studied with various versions of dispersion correction and solvation formulation. For the DFT methods, two dispersion / van der Waals corrected variants of the PBE[102] functional were used, namely ZORA-PBE-D4(EEQ)[54] and the ZORA-PBE-MBD@rsSC[56] / (all electron) TZP / COSMO(DCE) that differ by the construction of their dispersion force treatment, which may induce slight differences in the thermodynamics of association of extended molecular systems.

Note that the computed enthalpy of explicit solvation of **2**$^+$ by three molecules of DCE in COSMO(DCE) is exothermic and amounts to -9.5 kcal/mol with a Gibbs free energy of +27.3 kcal/mol (@PBE-D4(EEQ)). Thus, by virtue of the law of mass action, the explicit interaction of the solvent cannot be eluded.
Three situations were hence considered:

a) the implicit solvation by ways of the standard COSMO model (Table 8),

b) the explicit + implicit solvation considering the competition of the Lewis base binding to the Te center with explicitly weakly Te-interacting DCE molecules (Table 8), i.e. one DCE molecule per available σ-hole, and

c) without the COSMO solvation by considering nonetheless the explicit DCE interaction (Table 9).

a) implicit solvation

At this level of solvation, the association of $OPPh_3$ molecules with **2**$^+$ is slightly endergonic, in contradiction with experimental observations (Table 6). The difference of enthalpy of the first association between the three 1:1 [**2**•*B*]$^+$ adducts falls below the DFT accuracy limit, seemingly suggesting that the three σ-holes have the same probability of hosting a Lewis base. The same observation still holds when considering the 1:2 adducts, suggesting that the position of the first associated Lewis base has no influence over the position of association of a second base. Moreover, these results suggest that the V_{max} value of the σ-hole does not condition the association enthalpy. The experimental data listed in Table 3 suggest that real solvation and counterion binding do indeed cancel roughly 80-90% of the stabilizing interaction energy that can be calculated by DFT for static models taken in the solvation COSMO model (Table 6).
To verify the influence of the type of dispersion correction on the divergence of computed thermodynamics from experimental ones, the results obtained with the D4(EEQ)[54] correction of the dispersion were compared with calculations with the same native DFT functional, i.e. PBE, but using instead the MBD@rsSCS[56, 57] correction for dispersion.
From the optimized structures obtained from D4(EEQ) and MBD@rsSCS-corrected PBE, no major differences were observed in the geometries of the adducts.

Again, no major differences between enthalpies of association for the two approaches were observed for 1:1 and 1:2 adducts [**2**•$OPPh_3$]$^+$ and [**2**•$(OPPh_3)_2$]$^+$ respectively; most values remaining within a 1-to-5 kcal/mol difference. The Gibbs energies of association diverged significantly though for the 1:3 adduct [**2**•$(OPPh_3)_3$]$^+$, with a higher overestimation of exergonicity with the D4(EEQ) model. If many-body correlation effects can be ruled out as the main source of discrepancy with experimental data for the 1:1 and 1:2 adducts, the MBD correction tends to less overestimate the Gibbs energies of association particularly for the 1:3 adduct.

b) implicit & explicit solvation

This hybrid solvation model introduces a competition between $OPPh_3$ and DCE for interacting with the Te center in the thermochemical balance: in the chosen model this entails that each solvent molecule (namely DCE) arbitrarily occupies one "free" σ-hole of the Te in **2**$^+$, while the COSMO(DCE) implicit solvation is kept active.

Table 6. Enthalpies and Gibbs free energies of association (in kcal/mol) of $OPPh_3$ (abbr. *B*) molecules with $\mathbf{2}^+$ at 298.15 K under implicit and implicit + explicit COSMO solvation (red circles materialize implicit solvation).

Implicit COSMO solvation **Implicit COSMO + Explicit solvation**

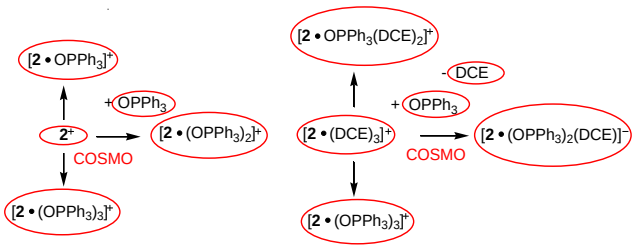

correction		-D4(EEQ)[a]		-MBD@rsSCS[a]	
adduct [b]	occupied σ-hole(s)	Δ*H*	Δ*G*	Δ*H*	Δ*G*
		implicit solvation (COSMO DCE)			
$[\mathbf{2}\bullet B]^+$	σ_1	-10	+5	-9	+7
	σ_2	-11	+3	-9	+7
	σ_3	-10	+2	-9	+5
$[\mathbf{2}\bullet B_2]^+$	$\sigma_{1,2}$	-23	+3	-25	+2
	$\sigma_{1,3}$	-24	+3	-26	+2
	$\sigma_{2,3}$	-24	+4	-25	0
$[\mathbf{2}\bullet B_3]^+$	$\sigma_{1,2},\sigma_3$	-46	-10	-41	0
		implicit solvation (COSMO DCE) + explicit DCE (1 per free σ-hole)			
$[\mathbf{2}\bullet B(DCE)_2]^+$	σ_1	-14	-8	-9	-2
	σ_2	-14	-9	-13	-6
	σ_3	-14	-7	-13	-8
$[\mathbf{2}\bullet B_2(DCE)]^+$	$\sigma_{1,2}$	-24	-16	*nc*[c]	*nc*[c]
	$\sigma_{1,3}$	-24	-14	*nc*[c]	*nc*[c]
	$\sigma_{2,3}$	-22	-17	-22	-15
$[\mathbf{2}\bullet B_3]^+$	$\sigma_{1,2,3}$	-39	-33	-34	-22

[a] computed at the ZORA-PBE-D4(EEQ) and ZORA-PBE-MBD@rsSC level of theory with an all electron TZP basis set, considering implicit or hybrid implicit/explicit solvation with COSMO (DCE) solvation [b] *B* = $OPPh_3$; [c] *nc*: not computed.

Table 6 shows that accounting for explicit molecules of solvent does not influence greatly the enthalpies of association of $OPPh_3$ with $\mathbf{2}^+$, whereas it significantly influences the Gibbs energies, evidencing the importance of the entropic factor. The hybrid implicit/explicit solvation approach predicts the associations of $OPPh_3$ with $\mathbf{2}^+$ to be exergonic; the second association being less favored than the first, which somewhat matches the experimental trend. Using the MBD@rsSCS correction for the dispersion instead of the D4 correction induces no significant variations of the geometries and only slight differences of the enthalpies and Gibbs free energies of association when applying the hybrid solvation approach. It is however noticed that for the formation of the adduct $[\mathbf{2}\bullet(OPPh_3)_3]^+$ the Gibbs free energy of association displays a difference of ca. -9 kcal/mol between the two models; the D4(EEQ) calculation overestimating again significantly the exergonicity of the 1:3 association.

c) explicit solvation in vacuum

Due to the large discrepancy between the D4 and MBD@rsSCS corrections for the 1:3 adduct, a deeper investigation of the impact of the dispersion/vdW corrections was necessary by removing the COSMO solvation.

Table 7. Enthalpies and Gibbs free energies of association (in kcal/mol) of $OPPh_3$ molecules (abbr. *B*) with $\mathbf{2}^+$ at 298.15 K in vaccuum and in vacuum with explicit DCE at various levels of dispersion – van der Waals corrections..

correction		-D4[a]	-TS[a]	-MBD@rsSCS[a]	-MBD-NL[a]
adduct[a]	occ. σ-hole	Δ*H*, Δ*G*	Δ*H*, Δ*G*	Δ*H*, Δ*G*	Δ*H*, Δ*G*
		vacuum			
$[\mathbf{2}\bullet B]^+$	σ_1	-30, -17	-30, -17	-28, -15	-28, -14
	σ_2	-29, -16	-29, -16	-27, -14	-27, -13
	σ_3	-30, -17	-31, -15	-28, -15	-28, -14
$[\mathbf{2}\bullet B_2]^+$	$\sigma_{1,2}$	-56, -30	-57, -28	-52, -26	-51, -25
	$\sigma_{1,3}$	-56, -29	-56, -29	-53, -27	-51, -24
	$\sigma_{2,3}$	-57, -29	-57, -29	-53, -26	-52, -25
$[\mathbf{2}\bullet B_3]^+$	$\sigma_{1,2,3}$	-83, -42	-84, -47	-77, -37	-74, -34
		partial explicit DCE (1 per free σ-hole)			
$[\mathbf{2}\bullet B]^+$	σ_1	-25, -21	-26, -22	-22, -18	-21, -17
	σ_2	-23, -19	-24, -20	-22, -18	-21, -17
	σ_3	-25, -20	-26, -20	-24, -19	-23, -19

[a] Computed at the ZORA-PBE-D4, ZORA-PBE-TS, ZORA-PBE-MBD@rsSCS and ZORA-PBE-MBD-NL levels of theory in the gas phase and with an all electron intermediate basis set and a partial explicit coordination of solvent molecules.

We thus compared the D4 pairwise correction,[54] the Tkatchenko-Scheffler (TS) pairwise approach, [55, 128] the range-separation self-consistent screening version of the many-body dispersion method (MBD@rsSCS) [56, 57, 128] and the non-local many-body dispersion method (MBD-NL)[58, 128] in the gas phase.[∞] Despite the error in total values of Δ*H* and Δ*G*, that is due to the expected over stabilization in gas phase compared to the solvent, there are consistent differences between the pairwise corrections and the many-body (MBD) ones, which are relevant for this work: as a matter of fact MBD@rsSCS and MBD-NL both increase the values of Δ*H* and Δ*G* (i.e. make them more positive).

The thermochemistry summarized in Table 7 shows a 1 to 2 kcal/mol agreement between TS and D4 corrections (both pairwise) for all the systems except for the large 1:3 adduct (namely here $[\mathbf{2}\bullet B_3]^+$), where the TS correction gives lower values of about 5 kcal/mol for ΔG. Both flavors of MBD are within 1 to 2 kcal/mol for the 1:1 and 1:2 adducts and within 3 kcal/mol for the 1:3 adduct for both enthalpies and the Gibbs free energies, with MBD-NL being always higher.

In fact, MBD-NL substantially improves the treatment of charge transfer and ionicity for vdW interactions compared to MBD@rsSCS.[58]

The many-body treatment of vdW interactions persistently leads to higher enthalpies and Gibbs free energies, when compared to the pairwise methods, with differences of 2 kcal/mol, 5 kcal/mol and 9 kcal/mol for the 1:1, 1:2 and 1:3 enthalpies respectively and of 3 kcal/mol, 4-5 kcal/mol and 8 kcal/mol for the 1:1, 1:2 and 1:3 Gibbs free energies respectively. Interestingly, MBD gives higher enthalpies and Gibbs free energies also in the case of the 1:2 adducts, where MBD@rsSCS calculations done using the COSMO implicit solvent model have the opposite trend.

The differences between pairwise and many-body vdW corrections in the gas phase can be explained by comparing the differences of the single point binding energies ΔE_0. The average differences $E_0 = E_0^{D4} - E_0^{MBD-NL}$ are of -2.5 kcal/mol, -5.1 kcal/mol and -8.6 kcal/mol for the 1:1, 1:2 and 1:3 adducts respectively. These differences increase almost linearly with the number of $OPPh_3$, persisting also for $\Delta\Delta H$ and $\Delta\Delta G$. The small deviations come mostly from the $\Delta\Delta E_0$ between $OPPh_3$ molecules, which we found to be of -0.7 kcal/mol and -2.0 kcal/mol for the 1:2 and 1:3 adducts respectively (cf. ESI, Table S22). We also find these results to be independent on the structural parameters, since almost the same energy differences $\Delta\Delta E_0$ are obtained using both the geometries obtained at -D4 or -MBD-NL levels.

Conclusion

This study investigates the affinity of a large variety of diarylmethyltelluronium cations towards various Lewis bases. It provides information on the thermodynamics of association, which complements the descriptive analysis of the XRD structures that in most cases shows that the Te center is indeed significantly Lewis acidic, which contributes to the crystal cohesion by numerous and varied interactions with the counterion.

By combining DOSY NMR and ITC, all carried out with solutions in an aprotic and moderate polar solvent, it is possible to approach the composition of the medium at various stoichiometries of a polar Lewis base such as $OPPh_3$. 1:1 and 1:2 telluronium-Lewis base associations could clearly be identified, except for ortho-aryl substituted telluroniums. It is also possible to extract rather accurately the enthalpies, the Gibbs free energies and constants of the first 1:1 association of a telluronium with a Lewis base while second and third association parameters are flawed with inherent ITC thermogram deconvolution limitations. One of them is that the deconvolution algorithms do not account for counterion's aggregation on the thermochemistry of the 1:2 and 1:3 associations. The diarylmethyltelluronium salts studied here display obvious dependency of their electrophilicity upon the nature of the substituents located at the aryl groups.

This dependency was sensed by ITC measures quite clearly from the investigation of the raw heats of association Q_{tot}, and proved particularly significant when the substituents of the Te-bound aryl fragment are two *meta* $-CF_3$ groups.

The dependency of the association thermochemistry on the nature of the counterion is now firmly established; it tends to support the fact that the origin and driving physical force of the interaction of neutral Lewis bases with the Te center is coulombic attraction, which is significantly screened by solvation.

Even though computed association ΔH and ΔG values lie far from experimental values, they give a gist of the extent of solvent's screening and entropic effects. Explicit solvation outlines indeed a significant solvent-dependent entropic contribution to the Gibbs free energy of association evidenced with the hybrid solvation model. Nonetheless the O-Te interaction in $[\mathbf{2}\bullet OPPh_3]^+$ bears a light covalent character that outlines that such chalcogen molecular complexes are nothing but a new class of Lewis type donor-acceptor complexes in which charge density transfer may be tuned by adjusting the electron-withdrawing properties of substituents either at the telluronium cation or the binding base.

IGM and IQA analyses clearly point to the dominant coulombic nature of the O-Te interaction, in which a weak but still significant covalent character is responsible for the charge density transfer occurring from $OPPh_3$ to the telluronium cation.

Last, it is found that pair-wise and many-body corrections offer similar performances on reproducing association energies of small to medium-large molecular complexes from the 1:1 to the 1:2 complexes of $\mathbf{2}^+$ with $OPPh_3$. However, for large molecular systems such as 1:3 assemblies, the MBD approach yields a lower over-stabilization of molecular complexes. This result suggests that the systematic trial of pair-wise vs. many-body corrections should be carried out for large assemblies containing extended or numerous π systems, this particularly when the closest match with experimental data is sought.

These results are timely in the current debate about the nature and directionality of the interactions involving σ-holes.[129] [47, 130] Cremer, Kraka *et al.*[131] already established the diversity of the interactions responsible for ChB. Our study points out the driving role of coulombic interactions and the weak contribution of covalence (charge transfer through constructive orbital interactions) in the formed molecular aggregates. Further developments will be disclosed in due time.

Supporting Information

Full experimental details on the synthesis & analyical characterizations, X-ray diffraction structural analyses, DOSY spectra, thermograms and thermodynamic parameters, geometries and energies of theoretically investigated structures are available in the SI. CCDC deposition numbers 2271927 (for **1a**), 2271911 (for **1c**), 2271918 (for **2a**), 2271928 (for **2b**),

2271925 (for **2c**), 2271917 (for **3a**), 2271919 (for **3b**), 2271923 (for **3c**), 2271913 (for **5a**), 2271914 (for **6a**), 2271930 (for **6b**), 2271929 (for **6e**), 2271912 (for **6f**), 2271915 (for **6h**), 2271922 (for **7a**), 2271926 (for **7b**), 2271920 (for **8a**, polymorph A), 2271916 (for **8a**, polymorph B), 2271924 (for **8b**), contain the supplementary crystallographic data for this paper. These data are provided free of charge by the joint Cambridge Crystallographic Data Centre and Fachinformationszentrum Karlsruhe Access Structures service.. The authors have cited additional references within the Supporting Information.[132-163]

Acknowledgements

Prof. Dr Stefan Grimme and Dr Andreas Hansen (University of Bonn) are thanked for their assistance in setting up effective DLPNO-CCSD(T) parameters. L.G. thanks the ANR for a PhD fellowship. The following institutions are thanked for their support: Centre national de la Recherche Scientifique, University of Strasbourg, Agence Nationale de la Recherche (ANR-21-CE07-0014), HPC center of the University of Strasbourg (grant g2022a202c), GENCI-IDRIS computing center (grant AD010812469R1), EXPLOR mesocentre (project 2021CPMXX2483).

Keywords: chalcogens • tellurium • calorimetry • density functional calculations • ab initio calculations

≠ The relative athermicity corresponds to the point in the titration where no significant heat flow occurs other than that caused by dilution or by the steady response of the chemical equilibrium to the addition of reagent by further injections of $OPPh_3$ solution.

¶ QTAIM[106] (including IQA) analyses and the determination of Bader atomic charges *q* were carried out for technical reasons with non-relativistic basis sets at the PBE0[164]/all electron TZP level with a 4*p* frozen core for Te. All other analyses, including the ADF-NCIPlot and IGM were carried out at the PBE-D4(EEQ) level stipulated above.

The IGM probes inter-fragment interactions in molecular or supramolecular systems based on the topology of the electron density. The IGM-based δg^{inter} descriptor compares the electron density gradient of the real system to the electron density gradient of the fictitious non-interacting system at any point of the real space, thus enabling a graphic visualization of "interaction maps" between two user-defined fragments by plotting isovalue surfaces. Integrating this descriptor over the whole real space yields the Δg^{inter} score which can be viewed as a measure of the electron sharing between the two user-defined fragments.

‡ The IBSI is an IGM-based atom-pair interaction descriptor to measure the strength of the interaction relative to the covalent case of H_2. The IBSI value can be used to classify the atom-pair interaction as noncovalent ($0\ a_0^{-1} <$ IBSI $< 0.15\ a_0^{-1}$), coordination ($0.15\ a_0^{-1} <$ IBSI $< 0.6\ a_0^{-1}$) or covalent (IBSI $> 0.15\ a_0^{-1}$).

∂ In the LED/DLPNO-CCSD(T) analysis the localized molecular orbitals are assigned to user-defined fragments based on Mülliken population analysis. The interaction energy is decomposed into an intra-fragment contribution $E^{(X)}_{intra} + E^{(Y)}_{intra}$, i.e. the contributions from pair of orbitals localized on the same fragment, (referred to as *electronic preparation* [99]) accounting for the variations of the electronic structure of one fragment induced by the presence of the other and an inter-fragment contribution $E^{(X,Y)}_{inter}$, i.e. the contributions from pair of orbitals localized on different fragments, accounting for the interaction of interest properly speaking: $\Delta E_{int} = E^{(X)}_{intra} + E^{(Y)}_{intra} + E^{(X,Y)}_{inter}$. The inter-fragment contribution can be partitioned into electrostatic $E^{(X,Y)}_{els}$, exchange $E^{(X,Y)}_{exc}$ and correlation $E^{(X,Y)}_{cor}$ contributions: $E^{(X,Y)}_{inter} = E^{(X,Y)}_{els} + E^{(X,Y)}_{exc} + E^{(X,Y)}_{cor}$. The intra-fragment contributions can be partitioned the same way. The inter-fragment correlation contribution can be further divided into charge transfer (double excitations changing the number of electron on each fragment $E^{(X,Y)}_{CT,X\to Y} + E^{(X,Y)}_{CT,Y\to X}$, dispersion (double excitations conserving the number of electron on each fragment $E^{(X,Y)}_{disp}$ and triple excitations: $E^{(X,Y)}_{(T)}$: $E^{(X,Y)}_{cor} = E^{(X,Y)}_{CT,X\to Y} + E^{(X,Y)}_{CT,X\to Y} + E^{(X,Y)}_{disp} + E^{(X,Y)}_{(T)}$.

∞ All calculations were undertaken with the FHI-aims code[128] using a state-of-the-art implementation, except for the calculations using the D4 pairwise corrections for which the *dftd4* package was used.[54]

[1] P. Politzer, P. Lane, M. C. Concha, Y. Ma, J. S. Murray, *J. Mol. Mod.* **2007**, *13*, 305-311.
[2] J. S. Murray, P. Lane, P. Politzer, *J. Mol. Model.* **2009**, *15*, 723-729.
[3] D. A. Decato, E. A. John, O. B. Berryman, in *Halogen Bonding in Solution*, **2021**, pp. 1-41.
[4] G. Cavallo, P. Metrangolo, R. Milani, T. Pilati, A. Priimagi, G. Resnati, G. Terraneo, *Chem. Rev.* **2016**, *116*, 2478-2601.
[5] M. S. Taylor, *Coord. Chem. Rev.* **2020**, *413*, 213270.
[6] S. Benz, M. Macchione, Q. Verolet, J. Mareda, N. Sakai, S. Matile, *J. Am. Chem. Soc.* **2016**, *138*, 9093-9096.
[7] P. Scilabra, G. Terraneo, G. Resnati, *Acc. Chem. Res.* **2019**, *52*, 1313-1324.
[8] R. E. Rosenfield, Jr., R. Parthasarathy, J. D. Dunitz, *J. Am. Chem. Soc.* **1977**, *99*, 4860-4862.
[9] J. Bamberger, F. Ostler, O. G. Mancheño, *ChemCatChem* **2019**, *11*, 5198-5211.
[10] A. Frontera, A. Bauza, *Int. J. Mol. Sc.* **2021**, *22*, 12550.
[11] S. Benz, J. López-Andarias, J. Mareda, N. Sakai, S. Matile, *Angew. Chem. Int. Ed.* **2017**, *56*, 812-815.
[12] P. Wonner, L. Vogel, M. Düser, L. Gomes, F. Kniep, B. Mallick, D. B. Werz, S. M. Huber, *Angew. Chem. Int. Ed.* **2017**, *56*, 12009-12012.
[13] P. Wonner, L. Vogel, F. Kniep, S. M. Huber, *Chem. Eur. J.* **2017**, *23*, 16972-16975.
[14] L. Vogel, P. Wonner, S. M. Huber, *Angew. Chem. Int. Ed.* **2019**, *58*, 1880-1891.
[15] N. Biot, D. Bonifazi, *Coord. Chem. Rev.* **2020**, *413*, 213243.
[16] S. Scheiner, *ChemPhysChem* **2023**, *24*, e202200936.
[17] W. Wang, B. Ji, Y. Zhang, *J. Phys. Chem. A* **2009**, *113*, 8132-8135.
[18] G. E. Garrett, G. L. Gibson, R. N. Straus, D. S. Seferos, M. S. Taylor, *J. Am. Chem. Soc.* **2015**, *137*, 4126-4133.
[19] P. Pale, V. Mamane, *ChemPhysChem* **2023**, *24*, e202200481.
[20] S. M. Walter, F. Kniep, L. Rout, F. P. Schmidtchen, E. Herdtweck, S. M. Huber, *J. Am. Chem. Soc.* **2012**, *134*, 8507-8512.
[21] A. Y. Bastidas Ángel, P. R. O. Campos, E. E. Alberto, *Org. Biomol. Chem.* **2023**, *21*, 223-236.
[22] K. Okuno, R. Nishiyori, S. Shirakawa, *Tetrahedron Chem* **2023**, *6*, 100037.
[23] Y. Lu, Q. Liu, Z.-X. Wang, X.-Y. Chen, *Angew. Chem. Int. Ed.* **2022**, *61*, e202116071.
[24] M. V. Il'in, A. S. Novikov, D. S. Bolotin, *J. Org. Chem.* **2022**, *87*, 10199-10207.
[25] X. He, X. Wang, Y.-L. Tse, Z. Ke, Y.-Y. Yeung, *Angew. Chem. Int. Ed.* **2018**, *57*, 12869-12873.
[26] X. He, X. Wang, Y.-L. S. Tse, Z. Ke, Y.-Y. Yeung, *ACS Catal.* **2021**, *11*, 12632-12642.
[27] Q. Zhang, Y.-Y. Chan, M. Zhang, Y.-Y. Yeung, Z. Ke, *Angew. Chem. Int. Ed.* **2022**, *61*, e202208009.
[28] R. Weiss, E. Aubert, P. Pale, V. Mamane, *Angew. Chem. Int. Ed.* **2021**, *60*, 19281-19286.
[29] B. Zhou, F. P. Gabbaï, *J. Am. Chem. Soc.* **2021**, *143*, 8625-8630.
[30] B. Zhou, F. P. Gabbaï, *Organometallics* **2021**, *40*, 2371-2374.
[31] K. Takagi, N. Sakakibara, S. Kikkawa, S. Tsuzuki, *Chem. Commun.* **2021**, *57*, 13736-13739.
[32] K. Takagi, N. Sakakibara, T. Hasegawa, S. Hayashi, *Macromolecules* **2022**, *55*, 3671-3680.
[33] L. Groslambert, A. Padilla-Hernandez, R. Weiss, P. Pale, V. Mamane, *Chem. Eur. J.* **2023**, *29*, e202203372.
[34] B. Zhou, F. P. Gabbaï, *Chem. Sci.* **2020**, *11*, 7495-7500.
[35] F. Heinen, E. Engelage, A. Dreger, R. Weiss, S. M. Huber, *Angew. Chem. Int. Ed.* **2018**, *57*, 3830-3833.

[36] R. Robidas, D. L. Reinhard, C. Y. Legault, S. M. Huber, *Chem. Rec.* **2021**, *21*, 1912-1927.

[37] R. J. Mayer, A. R. Ofial, H. Mayr, C. Y. Legault, *J. Am. Chem. Soc.* **2020**, *142*, 5221-5233.

[38] B. L. Murphy, F. P. Gabbaï, *J. Am. Chem. Soc.* **2023**, in press, doi:// 10.1021/jacs.1023c06991.

[39] M. Hall, D. B. Sowerby, *J. Organomet. Chem.* **1988**, *347*, 59-70.

[40] V. Mamane, P. Peluso, E. Aubert, R. Weiss, E. Wenger, S. Cossu, P. Pale, *Organometallics* **2020**, *39*, 3936-3950.

[41] R. Weiss, T. Golisano, P. Pale, V. Mamane, *Adv. Synth. Catal.* **2021**, *363*, 4779-4788.

[42] E. Aubert, A. Doudouh, E. Wenger, B. Sechi, P. Peluso, P. Pale, V. Mamane, *Eur. J. Inorg. Chem.* **2022**, e202100927.

[43] R. Weiss, E. Aubert, P. Peluso, S. Cossu, P. Pale, V. Mamane, *Molecules* **2019**, *24*, 4484.

[44] P. Pale, V. Mamane, *Chem. Eur. J.* **2023**, *n/a*, e202302755.

[45] F. Biedermann, H.-J. Schneider, *Chem. Rev.* **2016**, *116*, 5216-5300.

[46] D. J. Pascoe, K. B. Ling, S. L. Cockroft, *J. Am. Chem. Soc.* **2017**, *139*, 15160-15167.

[47] G. Haberhauer, R. Gleiter, *Angew. Chem. Int. Ed.* **2020**, *59*, 21236-21243.

[48] L. M. Grimm, S. Spicher, B. Tkachenko, P. R. Schreiner, S. Grimme, F. Biedermann, *Chem. Eur. J.* **2022**, *28*, e202200529.

[49] J. M. Schümann, L. Ochmann, J. Becker, A. Altun, I. Harden, G. Bistoni, P. R. Schreiner, *J. Am. Chem. Soc.* **2023**, *145*, 2093-2097.

[50] T. Clark, *J. Mol. Model.* **2023**, *29*, 66.

[51] J. Antony, S. Grimme, *Phys. Chem. Chem. Phys.* **2006**, *8*, 5287-5293.

[52] S. Grimme, *J. Comput. Chem.* **2006**, *27*, 1787-1799.

[53] S. Grimme, J. Antony, S. Ehrlich, H. Krieg, *J. Chem. Phys.* **2010**, *132*.

[54] E. Caldeweyher, S. Ehlert, A. Hansen, H. Neugebauer, S. Spicher, C. Bannwarth, S. Grimme, *J. Chem. Phys.* **2019**, *150*, 154122.

[55] A. Tkatchenko, M. Scheffler, *Phys. Rev. Lett.* **2009**, *102*, 073005.

[56] A. Ambrosetti, A. M. Reilly, R. A. DiStasio, A. Tkatchenko, *J. Chem. Phys.* **2014**, *140*, 18A508.

[57] A. Tkatchenko, R. A. DiStasio, R. Car, M. Scheffler, *Phys. Rev. Lett.* **2012**, *108*, 236402.

[58] J. Hermann, A. Tkatchenko, *Phys. Rev. Lett.* **2020**, *124*, 146401.

[59] R. Weiss, E. Aubert, L. Groslambert, P. Pale, V. Mamane, *Chem. Sci.* **2023**, *14*, 7221-7229.

[60] R. Weiss, E. Aubert, L. Groslambert, P. Pale, V. Mamane, *Chem. Eur. J.* **2022**, *28*, e202200395.

[61] R. Hoffmann, C. C. Levin, R. A. Moss, *J. Am. Chem. Soc.* **1973**, *95*, 629-631.

[62] F. Holtrop, K. W. Visscher, A. R. Jupp, J. C. Slootweg, in *Advances in Physical Organic Chemistry, Vol. 54* (Eds.: I. H. Williams, N. H. Williams), Academic Press, **2020**, pp. 119-141.

[63] G. Gryn'ova, C. Corminboeuf, *Beilstein J. Org. Chem.* **2018**, *14*, 1482-1490.

[64] J. P. Wagner, P. R. Schreiner, *Angew. Chem. Int. Ed.* **2015**, *54*, 12274-12296.

[65] R. Evans, *Prog. Nucl. Magn. Res. Spec.* **2020**, *117*, 33-69.

[66] R. Evans, Z. Deng, A. K. Rogerson, A. S. McLachlan, J. J. Richards, M. Nilsson, G. A. Morris, *Angew. chem. Int. Ed.* **2013**, *52*, 3199-3202.

[67] C. Bannwarth, S. Ehlert, S. Grimme, *J. Chem. Theor. Comput.* **2019**, *15*, 1652-1671.

[68] C. Bannwarth, E. Caldeweyher, S. Ehlert, A. Hansen, P. Pracht, J. Seibert, S. Spicher, S. Grimme, *WIREs Comput. Mol. Sci.* **2021**, *11*, e1493.

[69] A. Gervasini, in *Calorimetry and Thermal Methods in Catalysis* (Ed.: A. Auroux), Springer, Berlin, **2013**, pp. 175-195.

[70] J. A. Martinho Simoes, M. E. Minas da Piedade, *Molecular Energetics, Condensed-Phase Thermochemical Techniques*, Oxford University Press, New York, **2008**.

[71] Y. Marcus, G. Hefter, *Chem. Rev.* **2006**, *106*, 4585-4621.

[72] C. Hansch, A. Leo, R. W. Taft, *Chem. Rev.* **1991**, *91*, 165-195.

[73] R. Díaz-Torres, S. Alvarez, *Dalton Trans.* **2011**, *40*, 10742-10750.

[74] S. Alvarez, *Chem. Eur. J.* **2020**, *26*, 4350-4377.

[75] N. Takeda, T. Tagawa, M. Unno, *Heteroatom Chem.* **2014**, *25*, 628-635.

[76] C. A. Brautigam, H. Zhao, C. Vargas, S. Keller, P. Schuck, *Nat. Prot.* **2016**, *11*, 882-894.

[77] H. Duvvuri, L. C. Wheeler, M. J. Harms, *Biochemistry* **2018**, *57*, 2578-2583.

[78] F. Bou-Abdallah, M. R. Woodhall, A. Velázquez-Campoy, S. C. Andrews, N. D. Chasteen, *Biochemistry* **2005**, *44*, 13837-13846.

[79] C. Hammann, A. Cooper, D. M. J. Lilley, *Biochemistry* **2001**, *40*, 1423-1429.

[80] Y. Liu, G.-S. Chen, Y. Chen, D.-X. Cao, Z.-Q. Ge, Y.-J. Yuan, *Bioorg. Med. Chem.* **2004**, *12*, 5767-5775.

[81] T. Wiseman, S. Williston, J. F. Brandts, L.-N. Lin, *Anal. Biochem.* **1989**, *179*, 131-137.

[82] F.-G. Fontaine, D. W. Stephan, *Phil. Trans. R. Soc. A* **2017**, *375*, 20170004.

[83] F. W. B. Einstein, T. Jones, R. K. Pomeroy, P. Rushman, *J. Am. Chem. Soc.* **1984**, *106*, 2707-2708.

[84] Y. Cornaton, J.-P. Djukic, *Acc. Chem. Res.* **2021**, *54*, 3828-3840.

[85] S. Grimme, J.-P. Djukic, *Inorg. Chem.* **2010**, *49*, 2911-2919.

[86] G. Bistoni, A. A. Auer, F. Neese, *Chem. Eur. J.* **2017**, *23*, 865-873.

[87] E. W. Dahl, F. G. Baddour, S. R. Fiedler, W. A. Hoffert, M. P. Shores, G. T. Yee, J.-P. Djukic, J. W. Bacon, A. L. Rheingold, L. H. Doerrer, *Chem. Sci.* **2012**, *3*, 602-609.

[88] S. Grimme, J.-P. Djukic, *Inorg. Chem.* **2011**, *50*, 2619-2628.

[89] F. M. Bickelhaupt, E. J. Baerends, in *Reviews in Computational Chemistry*, **2000**, pp. 1-86.

[90] M. Mitoraj, A. Michalak, *Organometallics* **2007**, *26*, 6576-6580.

[91] R. F. W. Bader, *Atoms in Molecules: A Quantum Theory*, Oxford University Press, Oxford, **1990**.

[92] P. L. A. Popelier, *J. Mol. Model.* **2022**, *28*, 276.

[93] M. A. Blanco, A. M. Pendás, E. Francisco, *J. Chem. Theor. Comput.* **2005**, *1*, 1096-1109.

[94] V. Tognetti, L. Joubert, *ChemPhysChem* **2017**, *18*, 2675-2687.

[95] A. M. n. Pendás, M. A. Blanco, E. Francisco, *J. Chem. Phys.* **2004**, *120*, 4581-4592.

[96] J. Contreras-García, E. R. Johnson, S. Keinan, R. Chaudret, J.-P. Piquemal, D. N. Beratan, W. Yang, *J. Chem. Theor. Comput.* **2011**, *7*, 625-632.

[97] C. Lefebvre, H. Khartabil, J.-C. Boisson, J. Contreras-García, J.-P. Piquemal, E. Hénon, *ChemPhysChem* **2018**, *19*, 724-735.

[98] J. Klein, H. Khartabil, J.-C. Boisson, J. Contreras-García, J.-P. Piquemal, E. Hénon, *J. Phys. Chem. A* **2020**, *124*, 1850-1860.

[99] W. B. Schneider, G. Bistoni, M. Sparta, M. Saitow, C. Riplinger, A. A. Auer, F. Neese, *J. Chem. Theory Comput.* **2016**, *12*, 4778-4792.

[100] C. Riplinger, B. Sandhoefer, A. Hansen, F. Neese, *J. Chem. Phys.* **2013**, *139*, 134101.

[101] E. v. Lenthe, A. Ehlers, E.-J. Baerends, *J. Chem. Phys.* **1999**, *110*, 8943-8953.

[102] J. P. Perdew, K. Burke, M. Ernzerhof, *Phys. Rev. Lett.* **1996**, *77*, 3865-3868.

[103] A. Klamt, G. Schüürmann, *J. Chem. Soc., Perkin Trans. 2* **1993**, 799-805.

[104] M. V. Chernysheva, M. Bulatova, X. Ding, M. Haukka, *Cryst. Growth Des.* **2020**, *20*, 7197-7210.

[105] J. Lapp, S. Scheiner, *J. Phys. Chem. A* **2021**, *125*, 5069-5077.

[106] R. F. W. Bader, *Chem. Rev.* **1991**, *91*, 893-928.

[107] P. Jerabek, P. Schwerdtfeger, G. Frenking, *J. Comput. Chem.* **2019**, *40*, 247-264.

[108] C. Lefebvre, G. Rubez, H. Khartabil, J.-C. Boisson, J. Contreras-García, E. Hénon, *Phys. Chem. Chem. Phys.* **2017**, *19*, 17928-17936.

[109] E. G. Hohenstein, C. D. Sherrill, *WIREs Comput. Mol. Sci.* **2012**, *2*, 304-326.

[110] T. Schwabe, S. Grimme, J.-P. Djukic, *J. Am. Chem. Soc.* **2009**, *131*, 14156-14157.

[111] A. Li, H. S. Muddana, M. K. Gilson, *J. Chem. Theor. Comput.* **2014**, *10*, 1563-1575.

[112] C. Riplinger, P. Pinski, U. Becker, E. F. Valeev, F. Neese, *J. Chem. Phys.* **2016**, *144*, 024109.

[113] C. Riplinger, F. Neese, *J. Chem. Phys.* **2013**, *138*, 034106.

[114] D. G. Liakos, M. Sparta, M. K. Kesharwani, J. M. L. Martin, F. Neese, *J. Chem. Theory Comput.* **2015**, *11*, 1525-1539.

[115] T. Ziegler, A. Rauk, *Inorg. Chem.* **1979**, *18*, 1558-1565.

[116] R. Pollice, F. Fleckenstein, I. Shenderovich, P. Chen, *Angew. Chem. Int. Ed.* **2019**, *58*, 14281-14288.
[117] J. M. Schümann, J. P. Wagner, A. K. Eckhardt, H. Quanz, P. R. Schreiner, *J. Am. Chem. Soc.* **2021**, *143*, 41-45.
[118] A. Hansen, C. Bannwarth, S. Grimme, P. Petrović, C. Werlé, J.-P. Djukic, *ChemistryOpen* **2014**, *3*, 177-189.
[119] M. Hamdaoui, M. Ney, V. Sarda, L. Karmazin, C. Bailly, N. Sieffert, S. Dohm, A. Hansen, S. Grimme, J.-P. Djukic, *Organometallics* **2016**, *35*, 2207-2223.
[120] M. R. Milovanović, Q. Dherbassy, J. Wencel-Delord, F. Colobert, S. D. Zarić, J.-P. Djukic, *ChemPhysChem* **2020**, *21*, 2136-2142.
[121] M. R. Milovanović, S. D. Zarić, Y. Cornaton, J.-P. Djukic, *J. Organomet. Chem.* **2020**, *929*, 121582.
[122] W. Iali, P. Petrović, M. Pfeffer, S. Grimme, J.-P. Djukic, *Dalton Trans.* **2012**, *41*, 12233-12243.
[123] M. R. Milovanović, M. Boucher, Y. Cornaton, S. D. Zarić, M. Pfeffer, J.-P. Djukic, *Eur. J. Inorg. Chem.* **2021**, *2021*, 4690-4699.
[124] A. Klamt, V. Jonas, *J. Chem. Phys.* **1996**, *105*, 9972-9981.
[125] M. Kabeláč, P. Hobza, V. Špirko, *Phys. Chem. Chem. Phys.* **2009**, *11*, 3885-3891.
[126] S. Spicher, S. Grimme, *J. Chem. Theor. Comput.* **2021**, *17*, 1701-1714.
[127] S. Grimme, *Chem. Eur. J.* **2012**, *18*, 9955-9964.
[128] V. Blum, R. Gehrke, F. Hanke, P. Havu, V. Havu, X. Ren, K. Reuter, M. Scheffler, *Comput. Phys. Commun.* **2009**, *180*, 2175-2196.
[129] F. Weinhold, *Molecules* **2023**, *28*, 3776.
[130] L. de Azevedo Santos, T. C. Ramalho, T. A. Hamlin, F. M. Bickelhaupt, *Chem. Eur. J.* **2022**, *29*, e202203791.
[131] V. Oliveira, D. Cremer, E. Kraka, *J. Phys. Chem. A* **2017**, *121*, 6845-6862.
[132] E. Pietrasiak, A. Togni, *Organometallics* **2017**, *36*, 3750-3757.
[133] R. Amorati, L. Valgimigli, P. Dinér, K. Bakhtiari, M. Saeedi, L. Engman, *Chem. Eur. J.* **2013**, *19*, 7510-7522.
[134] M. Oba, Y. Okada, M. Endo, K. Tanaka, K. Nishiyama, S. Shimada, W. Ando, *Inorg. Chem.* **2010**, *49*, 10680-10686.
[135] K. Tiefenbacher, H. Dube, D. Ajami, J. Rebek, *Chem. Commun.* **2011**, *47*, 7341-7343.
[136] R. Weiss, (University of Strasbourg), **2021**.
[137] *"M86-EXX229V1 APEX3 User Manual"*, Madison, USA, **2016**.
[138] G. Sheldrick, *Acta Cryst. A* **2015**, *71*, 3-8.
[139] G. Sheldrick, *Acta Cryst. C* **2015**, *71*, 3-8.
[140] A. Spek, *J. Appl. Cryst.* **2003**, *36*, 7-13.
[141] G. W. T. M. J. Frisch, H. B. Schlegel, G. E. Scuseria, M. A. Robb, J. R. Cheeseman, G. Scalmani, V. Barone, B. Mennucci, G. A. Petersson, H. Nakatsuji, M. Caricato, X. Li, H. P. Hratchian, A. F. Izmaylov, J. Bloino, G. Zheng, J. L. Sonnenberg, M. Hada, M. Ehara, K. Toyota, R. Fukuda, J. Hasegawa, M. Ishida, T. Nakajima, Y. Honda, O. Kitao, H. Nakai, T. Vreven, J. A. Montgomery, Jr., J. E. Peralta, F. Ogliaro, M. Bearpark, J. J. Heyd, E. Brothers, K. N. Kudin, V. N. Staroverov, R. Kobayashi, J. Normand, K. Raghavachari, A. Rendell, J. C. Burant, S. S. Iyengar, J. Tomasi, M. Cossi, N. Rega, J. M. Millam, M. Klene, J. E. Knox, J. B. Cross, V. Bakken, C. Adamo, J. Jaramillo, R. Gomperts, R. E. Stratmann, O. Yazyev, A. J. Austin, R. Cammi, C. Pomelli, J. W. Ochterski, R. L. Martin, K. Morokuma, V. G. Zakrzewski, G. A. Voth, P. Salvador, J. J. Dannenberg, S. Dapprich, A. D. Daniels, Ö. Farkas, J. B. Foresman, J. V. Ortiz, J. Cioslowski, and D. J. Fox, Gaussian, Inc., Wallingford CT, **2009**.
[142] B. P. Pritchard, D. Altarawy, B. Didier, T. D. Gibson, T. L. Windus, *J. Chem. Inf. Model.* **2019**, *59*, 4814-4820.
[143] T. Lu, F. Chen, *J. Comput. Chem.* **2012**, *33*, 580-592.
[144] T. Lu, F. Chen, *J. Mol. Graph. Model.* **2012**, *38*, 314-323.
[145] G. te Velde, F. M. Bickelhaupt, E. J. Baerends, C. Fonseca Guerra, S. J. A. van Gisbergen, J. G. Snijders, T. Ziegler, *J. Comput. Chem.* **2001**, *22*, 931-967.
[146] E. Van Lenthe, E. J. Baerends, *J. Comput. Chem.* **2003**, *24*, 1142-1156.
[147] E. Francisco, A. Martín Pendás, M. A. Blanco, *J. Chem. Theor. Comput.* **2006**, *2*, 90-102.
[148] M. P. Mitoraj, A. Michalak, T. Ziegler, *J. Chem. Theor. Comput.* **2009**, *5*, 962-975.
[149] C. Lefebvre, J. Klein, H. Khartabil, J.-C. Boisson, E. Hénon, *J. Comput. Chem.* **2023**, *44*, 1750-1766.
[150] F. Neese, F. Wennmohs, U. Becker, C. Riplinger, *J. Chem. Phys.* **2020**, *152*.
[151] J. Zheng, X. Xu, D. G. Truhlar, *Theor. Chem. Acc.* **2011**, *128*, 295-305.
[152] F. Weigend, *J. Comput. Chem.* **2008**, *29*, 167-175.
[153] A. Altun, M. Saitow, F. Neese, G. Bistoni, *J. Chem. Theor. Comput.* **2019**, *15*, 1616-1632.
[154] A. Hjorth Larsen, J. Jørgen Mortensen, J. Blomqvist, I. E. Castelli, R. Christensen, M. Dułak, J. Friis, M. N. Groves, B. Hammer, C. Hargus, E. D. Hermes, P. C. Jennings, P. Bjerre Jensen, J. Kermode, J. R. Kitchin, E. Leonhard Kolsbjerg, J. Kubal, K. Kaasbjerg, S. Lysgaard, J. Bergmann Maronsson, T. Maxson, T. Olsen, L. Pastewka, A. Peterson, C. Rostgaard, J. Schiøtz, O. Schütt, M. Strange, K. S. Thygesen, T. Vegge, L. Vilhelmsen, M. Walter, Z. Zeng, K. W. Jacobsen, *J. Phys.: Cond. Matter* **2017**, *29*, 273002.
[155] V. Havu, V. Blum, P. Havu, M. Scheffler, *J. Comput. Phys.* **2009**, *228*, 8367-8379.
[156] M. Barborini, https ://github.com/QMeCha, **2023**.
[157] M. Burkatzki, C. Filippi, M. Dolg, *J. Chem. Phys.* **2007**, *126*.
[158] R. A. Kendall, T. H. Dunning, Jr., R. J. Harrison, *J. Chem. Phys.* **1992**, *96*, 6796-6806.
[159] D. E. Woon, T. H. Dunning, Jr., *J. Chem. Phys.* **1993**, *98*, 1358-1371.
[160] M. Marchi, S. Azadi, M. Casula, S. Sorella, *J. Chem. Phys.* **2009**, *131*.
[161] M. Casula, C. Attaccalite, S. Sorella, *J. Chem. Phys.* **2004**, *121*, 7110-7126.
[162] M. Barborini, A particle by particle size-extensive cut-off private communication.
[163] A. Zen, J. G. Brandenburg, J. Klimeš, A. Tkatchenko, D. Alfè, A. Michaelides, *Proc. Natl Acad. Sci.* **2018**, *115*, 1724-1729.
[164] M. Ernzerhof, G. E. Scuseria, *J. Chem. Phys.* **1999**, *110*, 5029-5036.

Entry for the Table of Contents

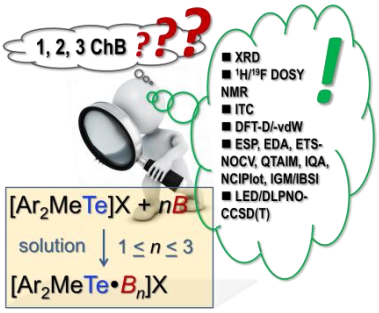

Telluronium salts $[Ar_2MeTe]X$ were synthesized and their Lewis acidic properties towards a number of bases were addressed in solution by physical and theoretical means; DFT and *ab initio* methods reveal the driving role of Coulombic and dispersion interactions in the formation of $[Ar_2MeTe{\bullet}B_n]^+$ complexes in solution (*B*= Lewis base).